THE ADVANTAGES OF COLLIMATOR OPTIMIZATION FOR INTENSITY MODULATED RADIATION THERAPY

by

Brian Doozan

A Dissertation Submitted to the Faculty of

The Charles E. Schmidt College of Science

In Partial Fulfillment of the Requirements for the Degree of

Doctor of Philosophy

Florida Atlantic University

Boca Raton, Florida

May 2017

THE ADVANTAGES OF COLLIMATOR OPTIMIZATION FOR

INTENSITY MODULATED RADIATION THERAPY

by

Brian Doozan

This dissertation was prepared under the direction of the candidate's dissertation advisor, Dr. Theodora Leventouri, Department of Physics, and has been approved by the members of his supervisory committee. It was submitted to the faculty of the Charles E. Schmidt College of Science and was accepted in partial fulfillment of the requirements for the degree of Doctor of Philosophy.

SUPERVISORY COMMITTEE:

Theodora Leventouri, Ph.D.
Dissertation Advisor

Silvia Pella, Ph.D., DABR

Korey Sorge, Ph.D.

John S. Faulkner, Ph.D.

George Malcolm Stocks, Ph.D.

Luc T. Wille, Ph.D.
Chair, Department of Physics

Ata Sarajedini, Ph.D.
Dean, Charles E. Schmidt
College of Science

Deborah L. Floyd, Ed.D.
Dean, Graduate College

April 4, 2017
Date

ABSTRACT

Author:	Brian Doozan
Title:	The Advantages of Collimator Optimization for Intensity Modulated Radiation Therapy
Institution:	Florida Atlantic University
Thesis Advisor:	Theodora Leventouri, Ph.D.
Degree:	Doctor of Philosophy
Year:	2017

The goal of this study was to improve dosimetry for pelvic, lung, head and neck, and other cancers sites with aspherical planning target volumes (PTV) using a new algorithm for collimator optimization for intensity modulated radiation therapy (IMRT) that minimizes the x-jaw gap (CA_X) and the area of the jaws (CA_A) for each treatment field.

A retroactive study on the effects of collimator optimization of 20 patients was performed by comparing metric results for new collimator optimization techniques in *Eclipse* version 11.0. Keeping all other parameters equal, multiple plans are created using four collimator techniques: CA_0, all fields have collimators set to 0°, CA_E, using the Eclipse collimator optimization, CA_A, minimizing the area of the jaws around the PTV, and CA_X, minimizing the x-jaw gap. The minimum area and the minimum x-jaw angles are found by evaluating each field beam's eye view of the PTV with *ImageJ* and finding the desired parameters with a custom script. The evaluation of the plans included the

monitor units (MU), the maximum dose of the plan, the maximum dose to organs at risk (OAR), the conformity index (CI) and the number of fields that are calculated to split.

Compared to the CA_0 plans, the monitor units decreased on average by 6% for the CA_X method with a p-value of 0.01 from an ANOVA test. The average maximum dose remained within 1.1% difference between all four methods with the lowest given by CA_X. The maximum dose to the most at risk organ was best spared by the CA_A method, which decreased by 0.62% compared to the CA_0. Minimizing the x-jaws significantly reduced the number of split fields from 61 to 37.

In every metric tested the CA_X optimization produced comparable or superior results compared to the other three techniques. For aspherical PTVs, CA_X on average reduced the number of split fields, lowered the maximum dose, minimized the dose to the surrounding OAR, and decreased the monitor units. This is achieved while maintaining the same control of the PTV.

ACKNOWLEGEMENTS

This research would not be possible without the help and support of the people at Florida Atlantic University (FAU) as well as those who work at South Florida Radiation Oncology (SFRO). Without the guidance of Dr. Silvia Pella, Ph.D., DABR of SFRO, I would not have accomplished this and many other projects. She allowed me to be able to explore the field of Medical Physics and was always available to any student who was willing to take the time to learn. I am truly grateful for her guidance and mentorship.

I would also like to personally acknowledge my second Dissertation Advisor, Dr. Th. Leventouri, Ph.D. Professor of Physics and Director of the Medical Physics program. She is the heart of the Medical Physics program at FAU and without her extensive efforts to build the program, none of this would have been possible. She has a door that is always open and assists in solving any problems that come my way.

I would like to thank Scott Whalen for his help in finding solutions to the optimizations presented here, Tom Costantino and David Littlejohn for their continued support and guidance with dosimetry, and Dan and Alysha Hodges for their comments on the details presented in this dissertation. I am grateful for the help from South Florida Radiation Oncology dosimetrists and staff for their time and the resources that they donated.

THE ADVANTAGES OF COLLIMATOR OPTIMIZATION FOR INTENSITY MODULATED RADIATION THERAPY

TABLES

FIGURES

1. INTRODUCTION

1.1 Purpose

The goal of this study is to improve the collimator optimization when delivering a 6 MV external photon beam using intensity modulated radiation therapy (IMRT). Publications regarding the benefits of collimator optimization for IMRT treatments have shown contradictory results[1,2]. In this research, new collimator optimizations were created to investigate the difference these optimizations produce in treatment plans for pelvis, lung and head and neck cancer patients' data.

1.2 Cancer

According to the National Institute of Health, cancer is the second leading cause of death in the United States[3], while almost a quarter of all deaths are linked to cancer[4]. Cancer is a disease that causes aberrant growths, or tumors, to grow uncontrollably and can metastasize to different tissues in the body[5]. When the cells start to replicate, the growth can adversely affect the function of the organ[6]. There are over 100 types of cancers that resulted in the death of more than 8.2 million people worldwide in 2010 according to the World Health Organization[7]. The leading causes of cancer include obesity, tobacco, alcohol, and a lack of nutrition in the diet2.

Technology has advanced the medical practice of treating diseases in the United States[8]. A unique blend of physics and medicine has improved the treatment of cancer through the use of high energy charged particles and photons in radiation therapy[9]. About

half of all cancer patients at the time of this writing in the United States are being treated with the use of radiation[10].

There are two main types of radiation therapy used to treat patients: brachytherapy and external beam radiation. Brachytherapy is a short-ranged radiation that is derived from a radioactive isotope and delivered near the tumor site[11]. It is common to treat bone metastases from prostate cancer with injected radium or breast cavities by placing catheters so radioactive seeds can travel in the tumor bed and deliver a prescribed amount of radiation. External beam radiation is the process of using a linear accelerator to deliver high energy electrons and photons in a controlled manor directed at the site of interest.

In many radiation treatments, and especially with external photon beam therapy, the patient undergoes a computed tomography (CT) scan. The images are then used to reconstruct the tumor structure and the critical organs which subsequently will be used to generate a radiation treatment plan using software for the appropriate machines. The quality of the treatment that a patient receives is directly correlated to the capabilities of the planner and the treatment planning system that will generate the treatment plan. It is imperative to the patient safety that the optimal steps have been taken by the planner as well as the software that is being used to visualize and evaluate the dose to be delivered to the patient.

According to the American Cancer Society, the estimated number of new patient cases of cancer will exceed 1.6 million in the year 2016. In the same year, more than half a million deaths in the United States will occur[12]. There are more than 200 known types of cancer affecting every organ in the body[13].

The most deadly cancer is found in the lung[14]. More than 200,000 people in the United States are expected to be diagnosed with lung cancer and will account for about 27% of the deaths from all cancers according the American Lung Association[15]. The three most commonly found types of lung cancer include small cell lung cancer, non-small cell lung cancer and lung carcinoid tumors. About 85% of these are non-small cell lung cancer (NSCLC)[16].

With a better screening process and more advanced options for treating cancers, the rate of deaths from the disease has steadily decreased for both men and women since the year 2000 in the United States. In the U.S., the age adjusted rate of death per 100,000 in the year 2000 is recorded to be 199.6 and fell steadily to a rate of 173.2 by 2009[17]. As the number of deaths from cancer decline, the number of cancer survivors has increased, which shows evidence that the medical advances have been successful in treating the disease[18].

1.3 Radiation Treatment

There are several modalities of radiation therapy that show evidence of being effective in treating lesions in the lungs[19]. The idea remains the same in the treatment methods in that they all use radiation from either a radioactive isotope or other means to break the DNA strands of the tumor cells in order to render them sterile. The type of radiation treatment generally depends on the size, location, and stage of the cancer. For lung lesions, the modality of radiation treatment consists of a stereotactic radiosurgery (SRS), stereotactic body radiotherapy (SBRT), intensity modulated radiation therapy (IMRT) with or without gating, conventional radiation therapy, or in a few patient cases, high dose rate (HDR) brachytherapy[20]. The dose is measured in the unit of Gray (Gy). One Gray equals an absorbed joule of energy per kilogram of mass.

Radiation therapy offers advantages either alone or in combination with chemotherapy or surgery compared to treatments utilizing only chemotherapy or surgery[21]. Radiation for prostate cancer can reduce side effects from a prostectomy including erectile dysfunction, urinary incontinence, or bleeding and infection from surgery[22]. For non-small cell lung cancer, chemoradiation is shown to give statistically significant benefits for the survival rates over chemotherapy alone and allows for treatment in areas of the lung deemed inoperable[23]. For head and neck cancers, the advancement of radiotherapy has become the standard to control the microscopic disease with or without surgery[24].

1.4 Linear Quadratic Model

The basic principle of radiation therapy is killing off tumor cells while sparing enough normal tissue as to not destroy the function of the surrounding organs. It is this reason that modeling how cells respond to radiation and fractionation scheduling is crucial to the development of radiotherapy. Of the several models that outline the cell survival curves, the fundamental plot is the linear quadratic model[25].

Radiation causes damage to the structure of the DNA in a cell. In a single hit theory, one electron will cause a double strand break in the DNA and result in damage that is irreparable, then the cell will cease to proliferate and necrose. The sterilization of all tumor cells is necessary for the procedure to be considered a cure. If a single hit to the DNA will create a cell that can no longer proliferate in a large population of the cells, the amount of cells surviving after a dose D can be modeled as

$$S = e^{-\alpha D}, \tag{1}$$

where S is the cell survival fraction, α is the cell killing response due to a single hit measured in Gy^{-1} and D is the delivered dose in Gy.

In the double hit theory, two ionizing particles are needed to damage the DNA. The probability of each event will go proportionally to the dose and the probability that the events will both occur goes as the square of the dose. Putting both factors into the cell survival curve gives the linear quadratic model equation 2,

$$S = e^{-(\alpha D + \beta D^2)}. \quad (2)$$

The coefficient β is the cell killing response due to a double hit measured in Gy^{-2}. The ratio of the two coefficients is found by setting the two exponential terms equal, where the single hit and double hit produce the same amount of kills in a cell,

$$\alpha D = \beta D^2. \quad (3)$$

Using equation (3) and solving for the dose, the ratio of the single and double hit coefficients is found. The ratio $\frac{\alpha}{\beta}$ effectively determines the shape of the cell survival curve. This quantity, measured in *Gy,* is used to determine the biological effects of radiation.

Cells that respond slowly to radiation early have low $\frac{\alpha}{\beta}$ values. This can be caused from either having a low value of α or a high value of β. In either case, the cells are said to be late responding and will be less responsive at lower dose values. This is beneficial for most organs as generally the tissue will have low $\frac{\alpha}{\beta}$ values. Tumors tend to replicate quickly, leading to a higher $\frac{\alpha}{\beta}$ values. Consequently, these tumors have a lower cell

survival than the surrounding normal tissue[27]. The amount of cells that are still able to proliferate after radiation is known as the surviving fraction.

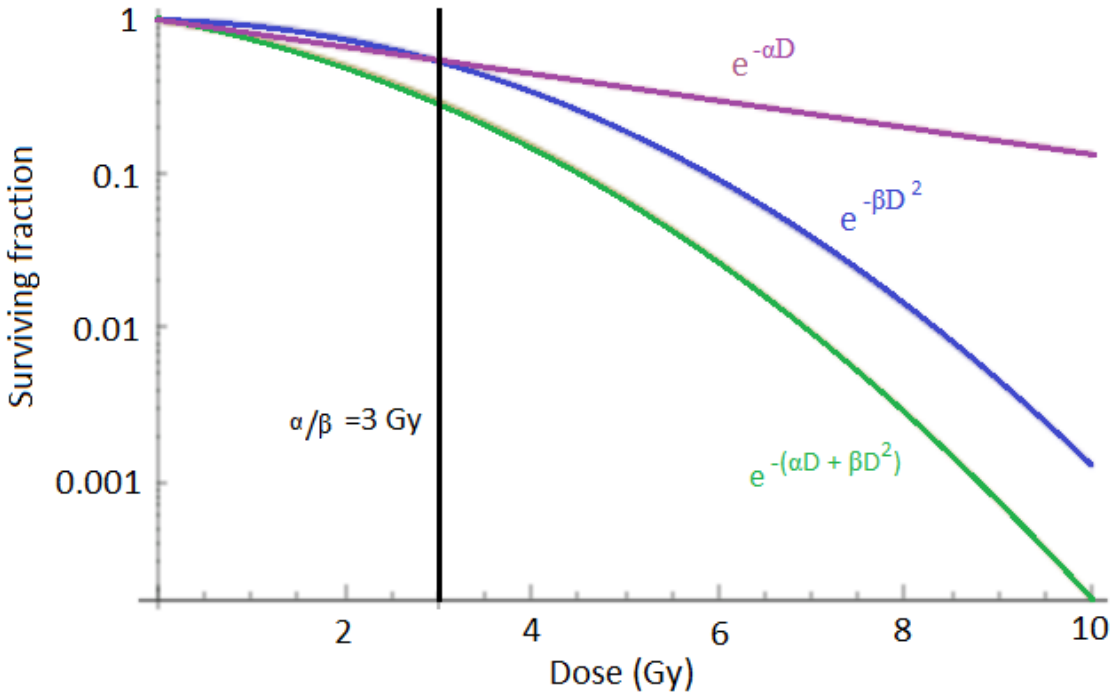

Figure 1: The linear quadratic (LQ) model shows the cell survival as a function of the dose delivered in a single fraction . The two components of the LQ model are made from the product of the single and double hit cell kill.

A lower $\frac{\alpha}{\beta}$ ratio indicates a late tissue response to radiation while higher ratios indicate an acute response[26]. Many tumors have a higher ratio than normal cells, although that is not always the case[26]. The importance of radiation is not always the total dose delivered, but the biological effect that a dose may have. Allowing time between treatments can be beneficial to give the superior control while inflicting less normal tissue damage.

1.5 Fractionation

Radiation therapy takes advantage of the different $\frac{\alpha}{\beta}$ ratios in tumors and surrounding normal tissue by giving fractionated low doses to allow the normal tissue to repair at a faster rate than the tumor volume[28]. A typical fractionation scheme, for example, would be to deliver 1.8 Gy for 25 fractions to the initial PTV and a boost treatment of 1.8 cGy for 18 fractions to the clinical tumor volume (CTV)[29].

Fractionation is beneficial because it will deliver the healthy normal tissue a sub-lethal dose of radiation and allow repair and repopulation before the next treatment. The hypoxic inner region of the tumor will also have time to oxygenate, which allows radiation to become more damaging to the cells[30]. The oxygenation allows for cells to go through mitosis more quickly and enhances the effects of radiation damage. Since tumor cells typically have higher $\frac{\alpha}{\beta}$ values, they respond early to the radiation. Normal surrounding tissues have lower $\frac{\alpha}{\beta}$ values and respond later to the therapy. The radiation "window of opportunity" typically peaks around 180 cGy, where the difference in the cell survival curve is the greatest between tumor cells and normal tissues. These radiobiological effects are important when determining the course of treatment for radiation.

To account for different types of radiation, response variation and fractionation schedules, a calculation of the biological effective dose (BED) is used to assess the biological dose that cells will receive. It is a helpful quantity that can be used to determine the remaining dose a tissue needs if there is a break in the delivery treatment or if a different type of radiation is being delivered. Conventional radiation treatment courses take weeks to months to complete and can result in tissues that regenerate and

repopulate. The tumor volume can be controlled by determining the amount of radiation that is required to deliver an effective dose to have the same biological effect.

The BED is computed for treatments that have any dose that is delivered over a course of days, weeks, or months. The survival curves that are used in radiation therapy are derived from treatment in a single dose. When cells are allowed time between the radiation, they will begin a process or repairing the DNA damage when a sub-lethal dose has been delivered[31]. It is then necessary to not evaluate purely on the absolute dose delivered, but the biological effective dose, which can be computed as

$$BED = nd\left(1 + \frac{d}{\alpha/\beta}\right), \tag{4}$$

where n is the number of fractions and d is the dose per fraction. The BED takes into account the $\frac{\alpha}{\beta}$ ratio, which is can be favorable for some lung carcinomas. In a study by William et. al., 4 out of 48 tumors were found to have $\frac{\alpha}{\beta}$ < 5 Gy, while the remaining tumors had values greater than 8 Gy. Many prostate tumors have low $\frac{\alpha}{\beta}$ between 1.5 and 4[33]. The low value is one reason why hypofractionation is implemented for patients with prostate cancer. Head and neck tumors were found to have $\frac{\alpha}{\beta}$ mostly above 10 Gy[35].

1.6 External Beam Radiation Therapy

External beam radiation therapy is regarded as an excellent source of treatment for a wide range of cancers. From skin lesion to a complicated volume around the spine, external beam radiation has been shown to have results that control the tumor with minimal side effects. Depending on the type of lesion being treated and the severity of the case, an array of sources can be used to give the optimal treatment.

The most conventional external beam device used in radiation therapy is a linear accelerator (LINAC). A LINAC, as in Figure 2, accelerates electrons, which can be used to treat superficial or skin cancers[36], or to create x-rays by inserting a metal target into the electron beam. The x-rays are then passed through a primary collimator to shape the beam into a cone. For conventional radiotherapy, a flattening filter is placed after the target to create a homogenous dose distribution. Some LINACS can opt to remove the filter to take advantage of the inhomogenous distribution for stereotactic radiosurgery using a flattening filter free (FFF) beam. The photon beam is shaped into a rectangular prism using two sets of jaws made of thick tungsten or other high atomic number material. The jaws are able to rotate with the collimator, allowing the rectangle to move in any orientation necessary. The last shaping of the x-rays uses a multi-leaf collimator (MLC). The MLC, which can be seen in Figure 3, is made up of high atomic number material in vertical sheets about 0.16 to 1.0 centimeter wide[37]. The leaves are able to transition in the x-direction independently to form a desired shape and can move during the treatment to change the delivery pattern to protect organs at risk (OAR). The number of leaves can vary depending on the manufacturer and model.

Figure 2: A cyberknife (left) and a truebeam (right) are examples of external beam linear accelerators (LINAC). The machines are able to move around the patient to target the PTV with x-rays.

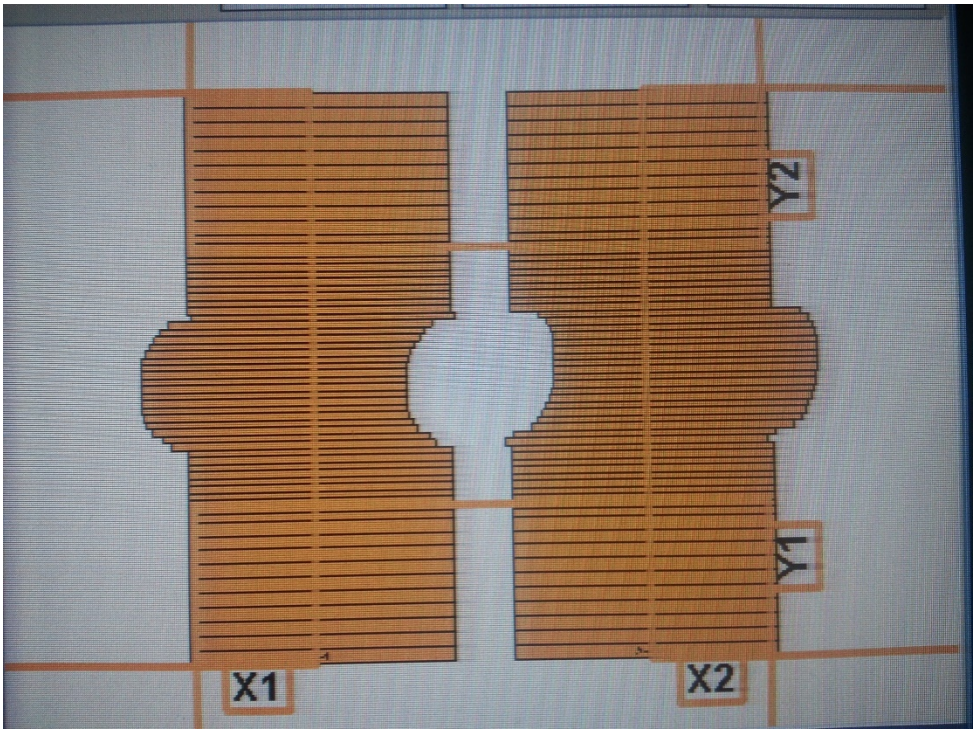

Figure 3: The multi-leaf collimator (MLC) is composed of two sets of leaves that modulate the dose by moving across the field in the x-direction. In this Varian 120 design, the inner leaves are 0.5 cm wide while the outer leaves are 1.0 cm.

The LINAC is composed of a gantry that can revolve around the treatment table and a collimator that rotates at the head of the gantry. The jaws and MLC are part of the collimator and rotate with it. There are two sets of jaws, an upper pair which movies in the y-direction and a lower jaw that moves in the x-direction for Varian machines. Additionally, the couch can rotate to provide an extra degree of freedom. For this study, the couch was fixed to a single position, while the gantry and collimator were used at different positions for treatment planning.

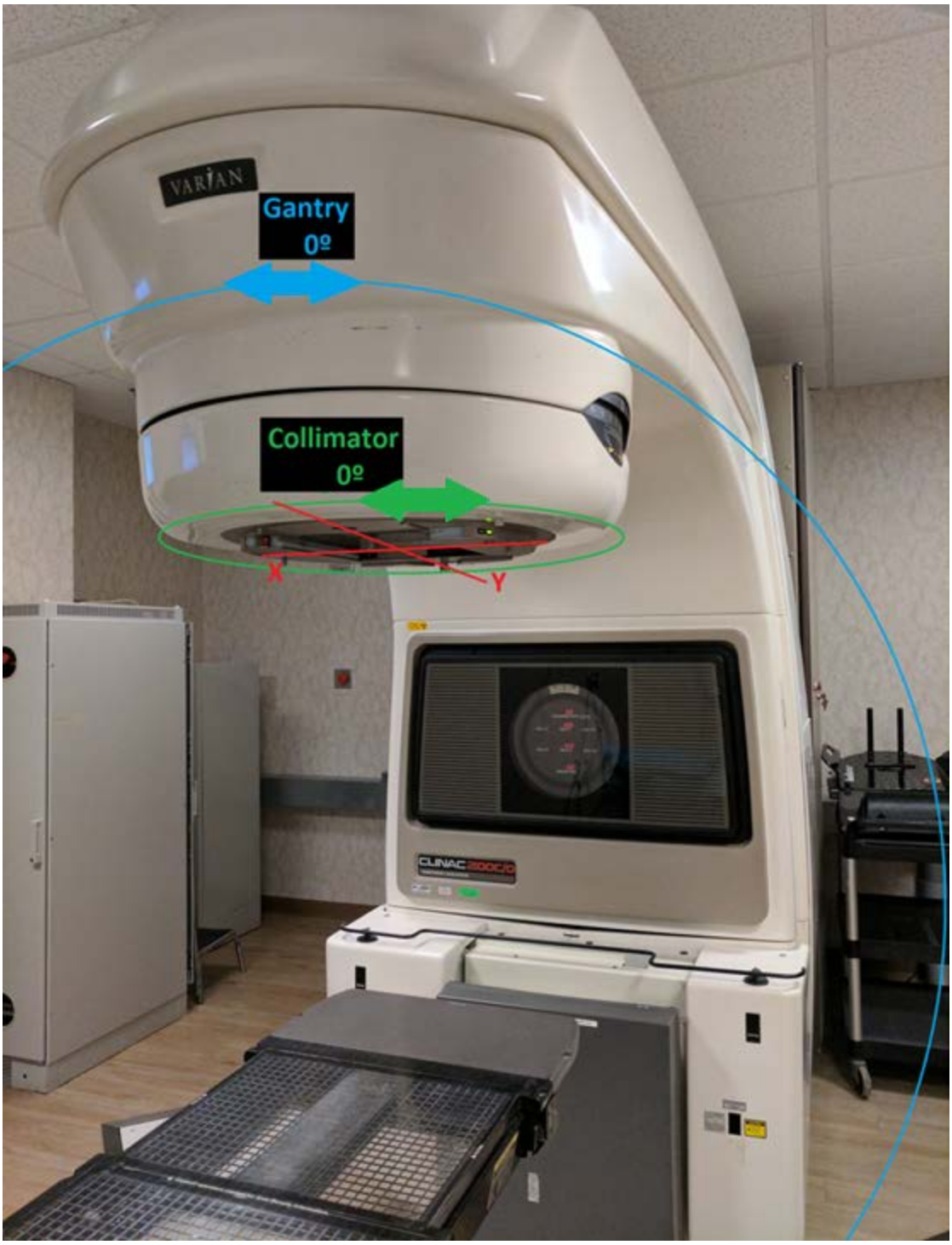

Figure 4: A LINAC showing the directions that the collimator (green) and gantry (blue) can move. The jaws and MLC are contained in the collimator and fixed to the angle of the collimator rotation. The set of x-jaws can travel only in the x-direction (red) and the set of y-jaws can travel along the y-axis. leaves on the MLC move in the x-direction.

1.7 Normal Tissue Complication and Tumor Control Probabilities

The most challenging aspect of radiation therapy is the side effect from radiating tissue around the tumor volume. The dose to the normal tissue is a consequence of the continuous dose deposition from photons. The curves shown in Figure 4 display the percentage depth dose for 6 MV and 15 MV photons incident in water. The initial increase in dose is useful in sparing the skin as electronic equilibrium has not yet been reached. Once equilibrium is reached, the dose will begin to decrease as attenuation and inverse-square factors take effect. The continuous dose distribution results in normal tissue surrounding the tumor in the line of the beam to receive a portion of the treatment radiation.

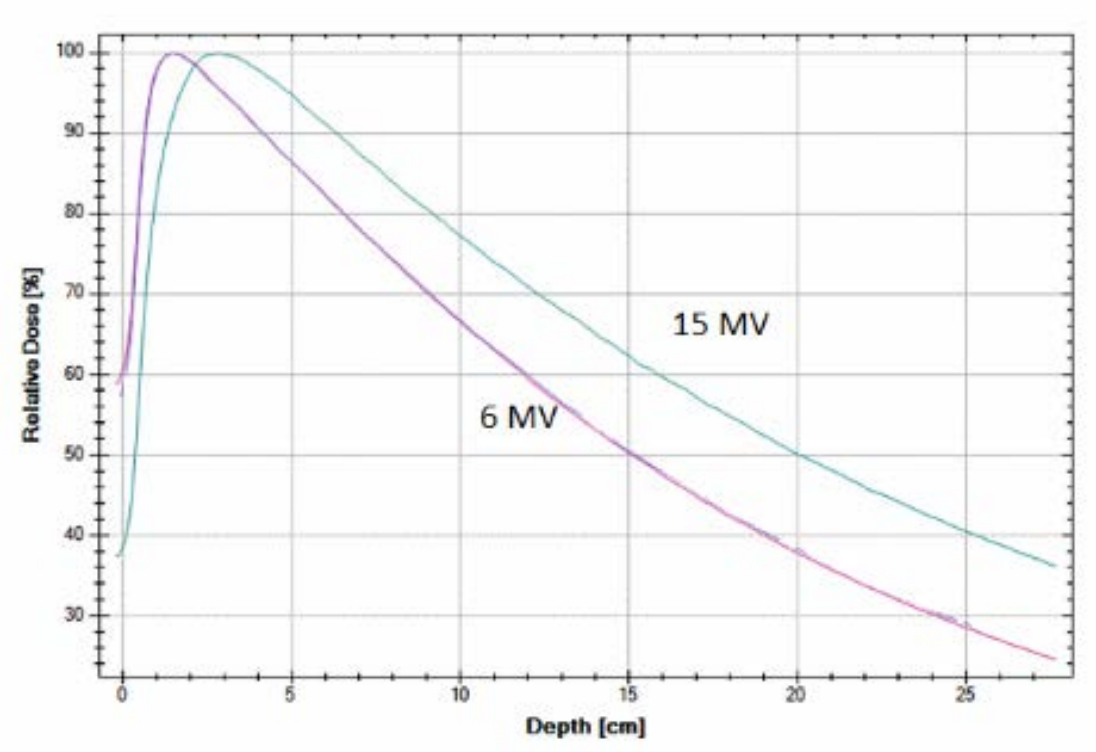

Figure 5: The percentage depth dose curves for 6 MV and 15 MV photons in water. The dose increases initially until electronic equilibrium is reached, and then falls off as the distance from the source increases. Since the dose is spread throughout the volume, the consequence to reach the target volume is that the surrounding tissue will also be irradiated.

The amount of radiation that tissue can tolerate depends on the type of organ. While no amount of radiation is recommended to any type of healthy tissue, the probability that an organ will develop complications increases with the amount of dose that it receives. The goal of radiation therapy is to deliver radiation that will control the tumor while limiting the complication of the normal tissue. Advances in technology with the MLC and algorithms used in treatment planning system have improved dose conformity and gradient to the PTV so that these goals may be achieved[38].

Delivering the amount of radiation to kill tumor cells is a relatively easy task. The challenge becomes limiting the dose in certain regions surrounding the PTV. The amount of radiation that the tumor volume receives will increase the tumor control probability (TCP), while the radiation that normal tissue will receive creates a normal tissue complication probability (NTCP). The two curves, illustrated in Figure 5, combines to form a window of opportunity, the uncomplicated tumor control probability, that will control a tumor while reducing the risk of normal tissue damage.

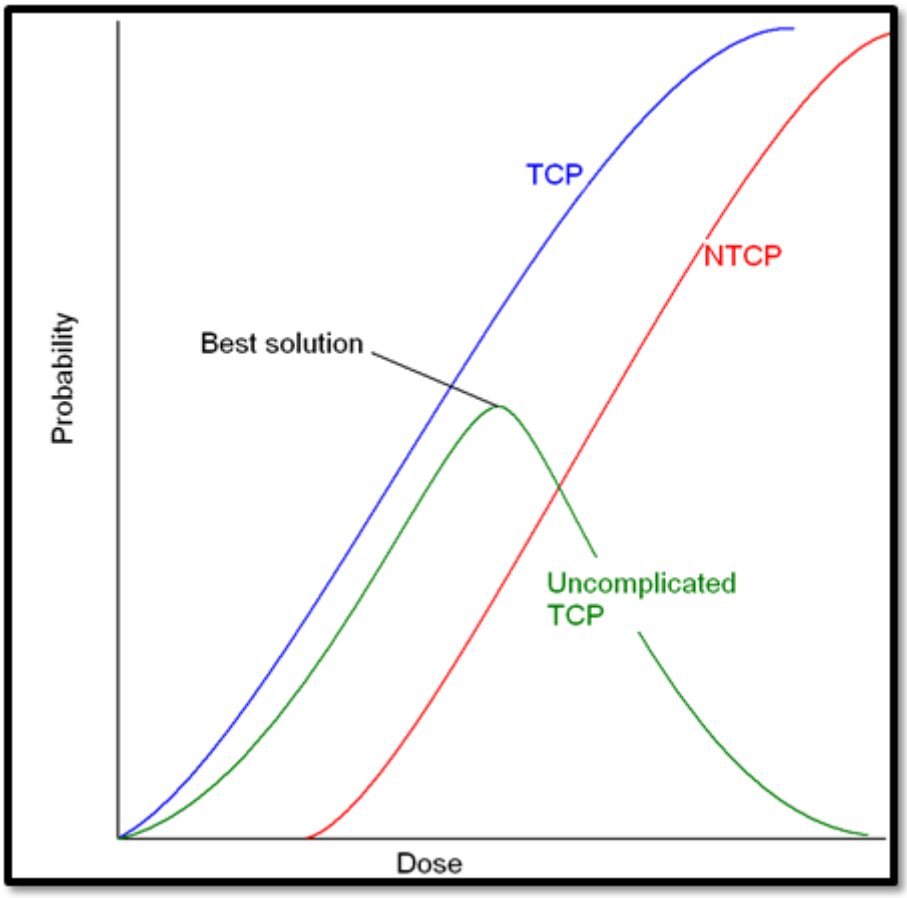

Figure 6: The tumor control probability (TCP) and the normal tissue complication probability (NTCP) curves both increase with dose. The uncomplicated TCP takes advantage of the radiosensitivity of tumor cells and provides a window of opportunity for radiotherapy planning. These models help with the guidelines for dose prescriptions around different organs of the body.

Organ failure occurs from radiation effects stochastically and nonstochastically. No amount of radiation is healthy and increasing the amount of dose to a healthy organ will also increase the risk of organ complications. Nonstochastic effects for the organs of the body are stored in databases of clinical trials. These empirical data have been analyzed by radiation oncologists to set standards for the amount of radiation that an organ can receive before showing nonstochastic effects.

Cancer cells are often more radiosensitive than the surrounding healthy tissue due to their rapid replication. Radiotherapy can take advantage of this, enabling better TCP

while reducing NTCP. Complications arise when this is not possible and a decision is made to either spare the function of an organ or to better control the target volume. These decisions are made in the practice of oncology and are met on an individual basis. As radiotherapy advances, these instances decrease as the ability to direct radiation more precisely increases. Improvement with patient localization also reduces the necessity for larger margins of uncertainty and less healthy tissue will overlap the PTV. Other forms of radiation such as protons can take advantage of sharp gradients of dose falloff to spare more tissue.

The NTCP model comes from a sigmoidal dose response curve that follows the equation

$$NTCP = \Phi\left(\frac{EUD - D_{50}}{mD_{50}}\right), \quad (5)$$

where $\Phi(x)$ is the probit function, m is the slope of the dose-response curve and D_{50} is the dose that would give a 50% chance of complication[39]. The equivalent uniform dose (EUD) is the amount of radiation an organ would receive if the total dose to the organ were uniformly distributed. This is used to determine the window of opportunity in developing plans that can control the tumor volume while maintaining functions of the organs surrounding it.

1.8 Treatment Planning

There are many variations of treatment planning systems (TPS) that are used for radiotherapy. The TPS used in this research was done in Eclipse version 11.0. For modern dosimetry, a patient first undergoes a computed tomography (CT) scan. The images are then imported into the planning system, where the Hounsfield units (HU) of

the CT scan of the patient are converted into electron density. The Figure 6 shows such a conversion from a CT scanner to a planning system. The electron densities are necessary for the planning algorithms to calculate the dose to the specific regions for a patient.

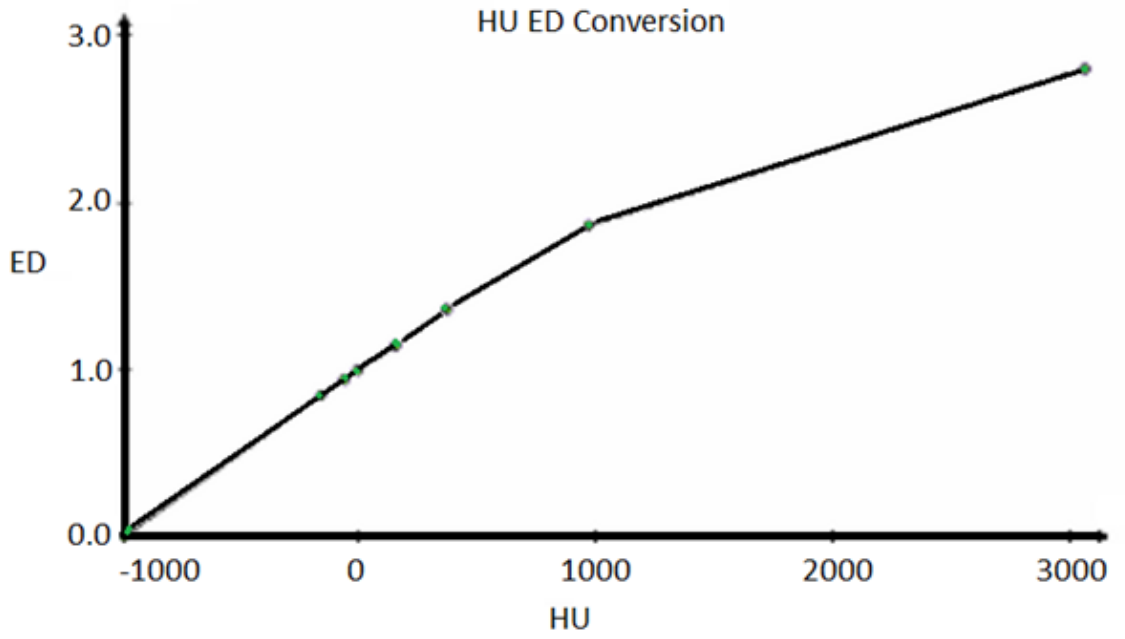

Figure 7: The graph showing a conversion from Hounsfield units (HU) to electron density. Planning systems use the electron density to calculate the 3D dose distribution throughout the patient volume.

The regions of interest (ROI) can be generated using an array of tools depending on the TPS. The contours can include organs at risk (OAR), target volumes, isodose volumes or other structures that can be used to control the dose gradient around the target, or OAR as in Figure 7**,** which displays a shell around the PTV. All of the contours can either be used as a portion of the target with a constraint to increase dose, an ROI or OAR with a constraint to limit the dose or a ROI with no constraints but can be used to evaluate the radiation. The OAR for a pelvic patient are displayed in Figure 8 which shows the femoral heads, bladder, rectum, prostate and bowel.

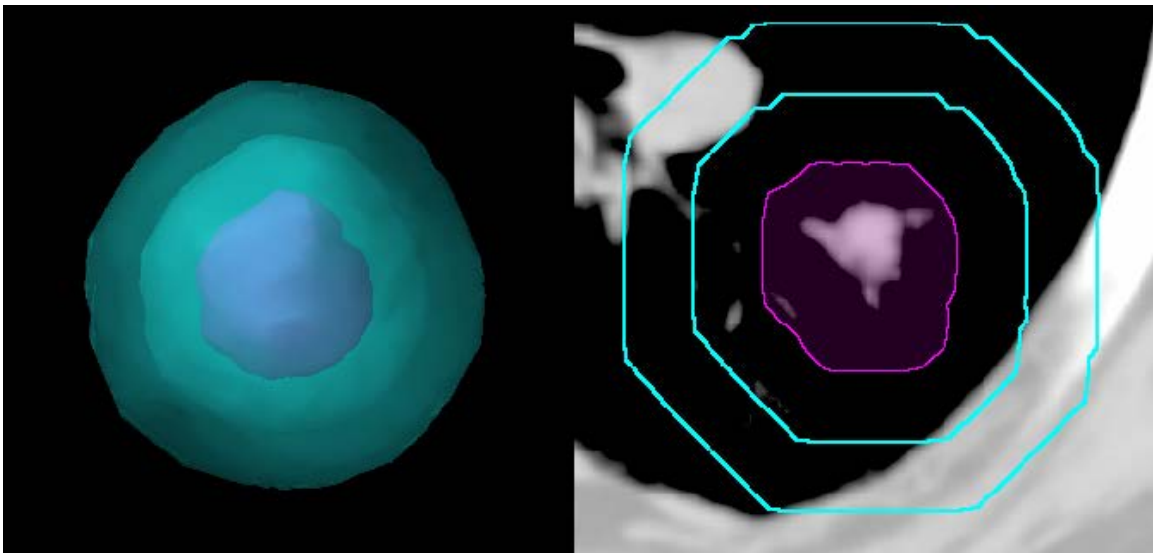

Figure 8: A target volume (purple) surrounded by a shell (cyan) in a 3D (left) view and transverse (right) view. Shells can be used as a constraint in planning to both assist in the dose gradient around the PTV and to to monitor isodose regions.

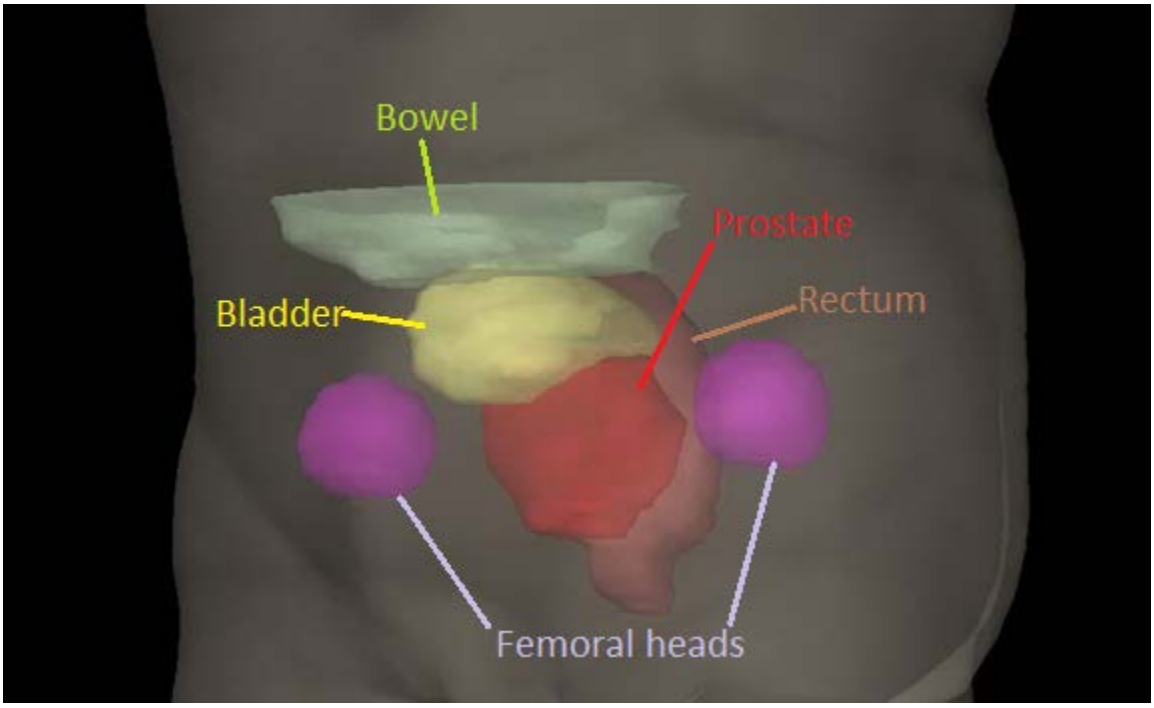

Figure 9: A 3D view of the organs for a pelvic patient which include the femoral heads, rectum, bladder, prostate and bowel. These are used as either target regions that have constraints to increase the dose or ROI that lower the dose. The advantage of IMRT is the ability to shape the radiation around regions of concern.

These parameters are used when developing the optimization for the plans. A TPS can have several modalities for delivering radiation. For IMRT, the dosimetrist has the choice in the number of fields that will be delivered and the collimator angle that each field will use. Often for IMRT treatment plans, the fields will be delivered at a single collimator angle. Once the fields are chosen for an IMRT plan, the optimization for inverse planning uses upper and lower objectives to define where the radiation will be delivered. These objectives are given weights depending on the importance of either the sensitivity of an organ or the amount of tumor control that must be met. In difficult cases of radiotherapy, a compromise between the amount of tumor control and normal tissue damage must be agreed upon with the radiation oncology team to determine a safe and effective treatment to be delivered.

The information from the constraints of the regions of interest are evaluated in a scoring function which when minimized gives the fluence model for each field. A simple scoring function can be written as

$$S = \sum_{i}^{n} w(Dose_{received} - Dose_{prescribed})_i^{\,2} + \sum_{j}^{m} w_j A_j (Dose_{received} - Dose_{allowable})_j^{\,2}, \quad (6)$$

where S is the total sum of the score, and the first summation is the value determined from the n voxel target regions. The weight factor w is chosen by the planner that can increase or decrease the TCP. The PTV region can be penalized in this type of function if any voxel in the PTV receives a dose greater than or less than the value of the prescription. The second summation is the value of all of the ROI which have constraints that limit dose, which typically would include organs or shells that are used for dose gradients. Each ROI can specify its own weight, w_j and is summed through the m voxels for each ROI. Since these regions are not targets, they are assigned a step function A_j,

where A_j is given the value of 1 when $Dose_{received} > Dose_{allowable}$ and 0 otherwise. While this type of scoring function works well to distribute the radiation to the target and away from the organs, it may be insufficient when evaluating the biological effects. The scoring function can be minimized by using either a simulated annealing or other gradient techniques that allows the process to escape local minima and find a global solution.

When the minimization of the scoring function is found, a fluence map for each beam is created that results in the desired dose distribution. Fluence is the 2D map made from the rectangle created, called a bixel, by the width of the leaves in the MLC and the distance that each leaf moves in one step. The amount of radiation that is delivered through each bixel and for each field will give the dose for each voxel in a patient plan. Lighter bixels in Figure 9 display regions that stay open longer as the leaves move across the area. The leaves on each side of the bixel move together along the x-axis to open and close the radiation field.

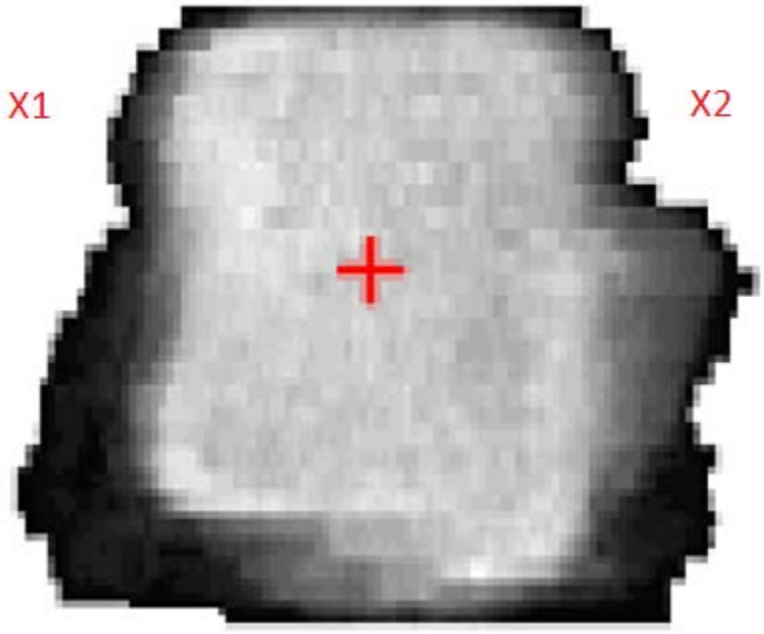

Figure 10: A fluence model displays bixels which corresponds to segments of varying lengths of radiation exposure. The lighter areas will have more exposure to radiation as the leaves move across the field from X1 to X2. Fluence models are used in radiotherapy to adjust the radiation to account for OAR which may be behind or in front of the target. Using multiple gantry angles allows for individual fluence maps to generate the dose for each voxel.

After a plan is optimized and has a fluence model calculated for leaf position, the plan can be shifted by a means of normalization. Normalizing plans will only scale the dose distribution and will not change the dose distribution. Similarly, changing the prescription or fraction dose will also scale the resulting dose. This can be useful in normalizing the dose to give a certain value of TCP and determining if adjustments must be made on the OAR to give a safe treatment to a patient.

1.8.1 Intensity Modulated Radiation Therapy Necessity

IMRT has advantages over conformal planning in that it allows for dose modulation to shape the isodose lines away from sensitive organs. For head and neck cases, for example, sensitive structures such as the parotid glands and spinal cord that are

sufficiently close, but outside of the PTV, require high dose gradients and dose shaping for additional safety and morbidity reduction related to radiation. It will also afford the greatest likelihood of local tumor control while significantly decreasing the probability of acute and chronic toxicity for the treatment of such malignancies. In such cases, IMRT allows for the maximum sparing of adjacent normal organs. In a head and neck case shown in Figure 10, the isodose lines for the 100, 90, and 80 percent of the prescription dose is shown along with the adjacent parotids and spinal cord. The outline shape of the isodose curves is manipulated, with the inverse planning technique to limit the dose to the critical structures while maintaining a high dose to the tumor volume. This type of treatment would be difficult to implement without the use of modulation of the MLC.

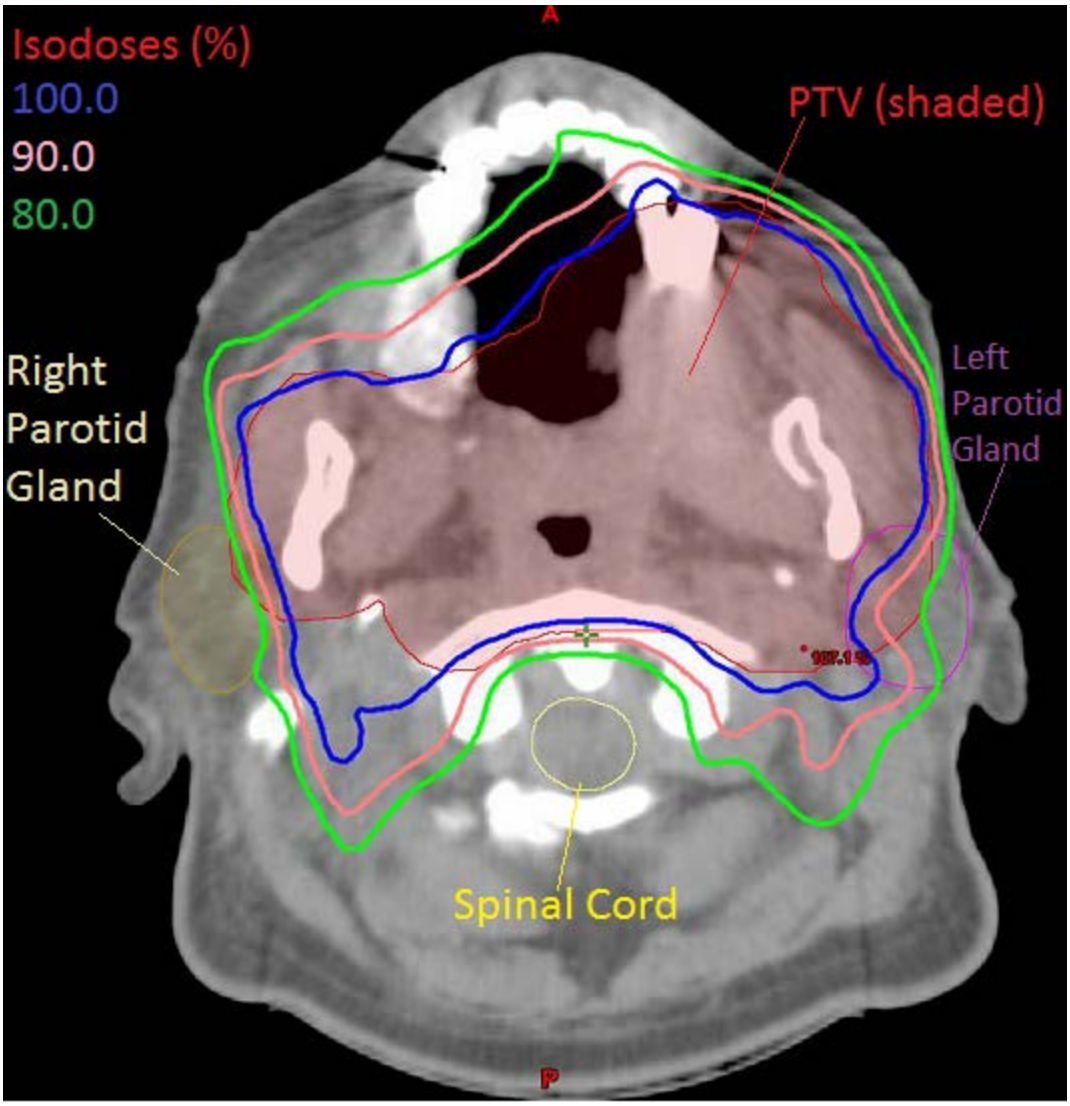

Figure 11: A head and neck case shows the advantage of IMRT planning. The isodose lines are able to shape around sensitive organs, allowing maximum coverage of the PTV while minimizing the risk of acute and chronic toxicity of the OAR.

1.9 Dose Calculations

The dose distribution in the TPS is calculated from the fluence generated in from the optimizations. Fluence for x-ray radiation is the number of photons passing through each bixel, which can be calculated with the equation

$$\phi = \frac{dN}{dA}, \tag{7}$$

where ϕ is the fluence, and N is the number of photons passing through the area A. If the energy is monoenergetic, then the energy fluence, $\Psi(E)$, can be written as the fluence times the energy of the beam,

$$\Psi(E) = \frac{dN}{dA}\mathrm{E} \tag{8}$$

$$\Psi(E) = \phi\, E. \tag{9}$$

The function $\Psi(E)$ is the fluence for photons of energy E. Radiotherapy uses a spectrum of photon energies which are created from the interaction of high energy electrons with a tungsten target. The particle fluence includes this energy spectrum from a LINAC and the energy fluence can be accounted for by taking the differential with the energy[39] as in the equations 10 and 11,

$$\phi_E(E) = \frac{d^2N(E)}{dAdE} \tag{10}$$

$$\phi_E(E) = \frac{d\phi(E)}{dE}. \tag{11}$$

This is equivalent to the summation of multiple energy fluence photons. For a LINAC defined at specific energies, and specifically 6 MV for the purpose of IMRT, the average energy of the spectrum is about a third of the maximum defined energy.

Since fluence is the number of particles through a bixel and the energy spectrum is known, the algorithms used can find the amount of energy that will be deposited in each voxel of the CT scan. Photons attenuate through interactions with matter and as they do so, the energy is transferred from the photon to the atoms it interacts with. The type of interaction that occurs depends on the energy of the photon, the density of the material and the effective atomic mass. These interactions can either result in little to no energy

loss by deflecting in Raleigh scattering or pair or triplet production[40]. For a clinical LINAC using IMRT, the most common type of photon interaction is from Compton scattering.

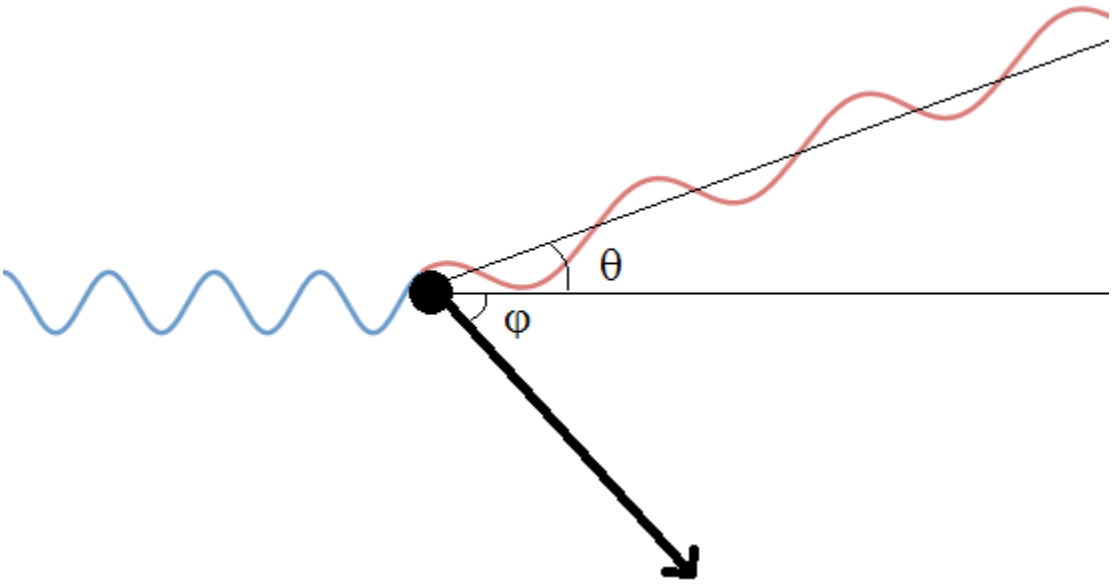

Figure 12: Compton scattering is the dominant type of photon interaction for LINAC based radiotherapy today. A photon is incident on a free electron and scatters at an angle θ. A recoil electron absorbs the energy that is lost from the collision of the photon.

Compton scattering, shown in Figure 11, is the inelastic scattering of photons off of electrons. The wavelength of the scattered photon increases with the angle, which decreases the energy of the photon and results in an increase of energy to the electron. The energy that is imparted to the electron from Compton scattering is part of the stopping power from the medium. The probability of interaction depends on the linear attenuation of the medium, μ, which is the sum of all the interaction modalities with Rayleigh scattering, photoelectric effect, Compton scattering and pair production

$$\mu = \mu_{Rayleigh} + \mu_{photoelectric} + \mu_{Compton} + \mu_{pair\ production}. \quad (12)$$

The total energy released per unit mass (TERMA) is the product of the mass attenuation coefficient (μ/ρ) of the matter and the fluence of the beam **Error! B ookmark not defined.**. The energy that is lost from the photons is absorbed by the electrons and either released with a second photon or transferred in a collision. The portion of the incident photon energy that is transferred to the charged particles of the material is the KERMA, or kinetic energy released per mass. This is the energy that is used to damage the DNA in the nucleus of cells and is what can treat cancer patients when released in tumor cells.

To successfully model this track of energy, approximations can be made to increase the efficiency of treatment planning systems to make the process clinically practical. One such approximation is the interaction of the photon as it attenuates through the medium. The continuous slowing down approximation (CSDA) range model simulates the tracks of electrons losing energy as they slow down and deposit energy through the motion. This type of calculation allows for the distance that an electron may travel through the tissue and calculate the energy that is delivered or the number of δ electrons that may escape. The range is thus calculated from the energy per stopping power as the integral

$$R_{CSDA} = \int_0^{E_{K_i}} \frac{dE}{S_{tot}(E)}, \tag{13}$$

where E_{K_i} is the initial energy of the photon and $S_{tot}(E)$ is the total stopping power of the medium as a function of the energy[41].

The dose that is calculated in the TPS depends on the exact algorithm that the system uses. This can be a pencil beam algorithm that quickly calculates an accurate dose

to heterogeneous tissue or variations of Monte Carlo algorithms that are widely accepted as the gold standard but take the most computational time. Most algorithms for treatment planning systems today fall in this spectrum. Often, a pre-calculated kernel is used as a convolution superposition, which will account for the TERMA. The kernels used range in complexity but can incorporate the same principles and use a Monte Carlo approximation to a good representation of the dose with a relatively fast calculation[42]. The dose to each coordinate voxel can then be calculated in a volumetric integral with dependencies on the fluence, mass attenuation coefficients, and the kernel as shown in equation 14 for a homogeneous scan[44]

$$D(x,y,z) = \iiint \frac{\mu}{\rho}\psi(x',y',z')K(x-x',y-y',z-z')dV'. \qquad (14)$$

The interactions occur at coordinates (x',y',z') and (x,y,z) are point coordinates where the energy is deposited.

1.10 Collimator Optimization

The Eclipse optimization, CA_E, is an option that can be used for both conformal planning and IMRT. The optimization chooses the best angle to fit the MLC leaves to the tumor volume. For the purpose of this study, the optimization was used along with three other methods in 20 plans for comparison with other methods of collimator rotations.

The default setting in Eclipse for IMRT treatment planning, CA_0, is keeping the collimator at an angle of 0 degrees for every field. This is the model that was as the standard in the study as it is frequently used to treat cancers of the pelvic, lung and head and neck regions with IMRT treatment planning. Other models have been published for testing the effectiveness in treating tumors with other variations of collimator rotations

and have found that keeping the collimator at fixed angles can have advantages in controlling the dose to surrounding normal tissue[43].

The new optimizations that are presented in this research, CA_A and CA_X, work by minimizing the area of the jaws and the x-jaw distance, respectively. These methods have advantages in either minimizing the area of the exposed radiation field for CA_A or by minimizing the distance that the leaves travel in the x-direction. The CA_X method also has the ability to minimize the number of fields that will split for a Varian accelerator.

1.11 Evaluating Dosimetry Plans

The treatment plans that are created for each patient are examined by an oncology team that can consist of dosimetrists, physicists, oncologists, and therapists. Each member of the team has been trained to evaluate different aspects of the plan. Important tools are helpful in evaluating the dosimetry of the plan, which would show what the contoured regions would receive if the plan was delivered perfectly. This is an ideal case as every patient's anatomy will change from day to day. The alignment of the patient, however careful, will always have deviations. The dose volume histogram (DVH) shows such a case where the OAR or PTV can be carefully analyzed as to what kind of radiation it will receive. The team can then decide the appropriate coverage of the tumor while minimizing the radiation effects for the surrounding tissue.

Evaluating the isodose lines throughout the volume of the scan is important to detect any hotspots, or regions of high dose, that may form away from the PTV. Often, these can be removed through manipulation of the dose constraints to the PTV and OAR or modifying the gantry positions, number of fields, collimator angle, or couch angle. These hotspots can cause damage to tissue far away from the PTV and increase side effects to the patient.

Other factors that are used in plan evaluation are the conformity index and the conformation number. The conformity index is the ratio of the prescription dose volume and the volume of the PTV. Ideally, these volumes will overlap. A ratio that is below 1 indicates incomplete coverage of the tumor with the prescription dose, while a ratio over 1 would be irradiating healthy tissue with the treatment dose. This ratio does not take into account the spatial position of where the treatment volume occurs. To correct for this, the conformation number can also be used. For this, the volume of the overlapping PTV and prescription dose is used with that of the prescription isodose volume and the volume of the PTV. Equations 15 and 16 show these indices,

$$CI = \frac{V_{100\%}}{\mathrm{TV}} \tag{15}$$

$$CN = \frac{TV_{RI}}{\mathrm{TV}} \times \frac{TV_{RI}}{V_{RI}}. \tag{16}$$

The variable $V_{100\%}$ is the volume covered by 100% of the prescription dose, TV_{RI} is the PTV volume intersected by the prescription dose, TV is the volume of the PTV and V_{RI} is the prescription isodose volume[45].

The limitation for the MLC in the tested Varian LINACs is the distance that the leaves are able to move before the ends are no longer covered by the jaws. This limit is about 14.5 cm. Any treatment field that covers a distance longer than 14.5 cm requires multiple carriage fields. The field will split to first cover a portion of the PTV before running a second field at the same gantry position. The second subfield will have a different position of the x-jaws and the leaves will cover the remainder of the PTV.

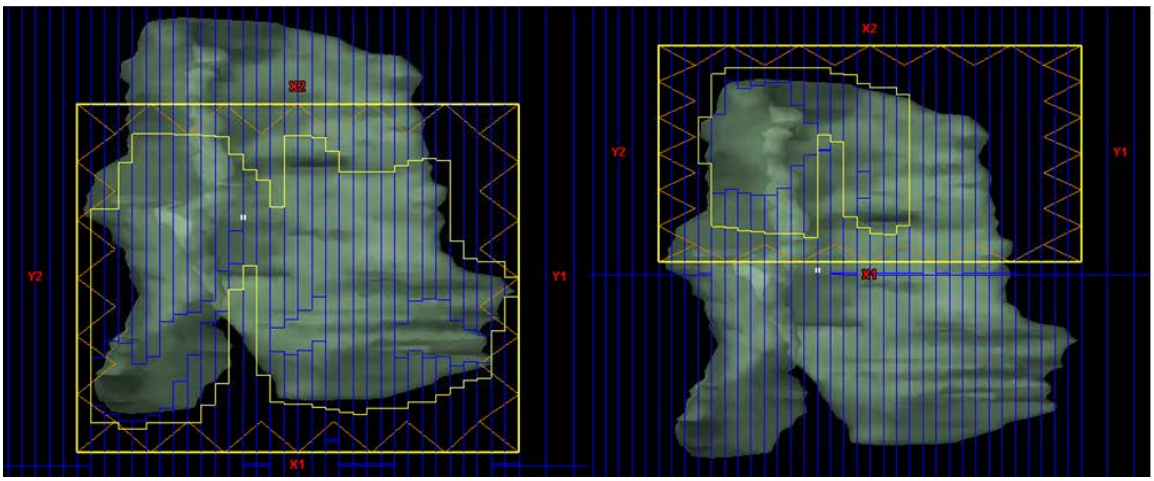

Figure 13: A field with an x-direction distance over the 14.5 cm limit of which the leaves can move requires two fields. The first field (left) will cover the lower portion of the PTV as the leaves (blue) move from across the area from X1 to X2. A second subfield (right) is required so that the X1 and X2 jaws move to a position that is sufficient for the MLC to safely move across.

Split fields can increase the time a patient is on the table, as well as the time it requires to verify a plan. Each field for a Varian machine was measured to require about 15 seconds additional time for each subfield, but this varies for each machine. In addition to time, the subfields have sharp dose falloff, which must be matched with the next field. The steep gradient can cause errors if a patient is out of position, causing either overlapping doses or a gap between fields. To minimize the split fields, gantry positions can be changed or the collimator can be rotated to possibly try to resolve the issue since the leaves will only move in the x-direction.

The delivery is also checked for IMRT cases by running a quality assurance (QA) plan on a device that can be cross checked with a predicted dose. Such tools include electronic portal imaging devices (EPID), MapCheck or other similar diode arrays. The QA can also include comparison log files that track the position of the leaves throughout the delivery with that of the calculated leaf motion. All of these are capable of comparing the planned file with how the LINAC will deliver the radiation. This check is important

for IMRT planning to ensure that the limitations of the LINAC will not be exceeded and the proper distribution of radiation is deliverable to the patient.

2. MATERIALS AND METHODS

2.1 Patient Selection

Twenty patient cases were selected that consisted of ten pelvic, five lung and five head and neck cancers. To be selected, a patient must have been planned in Eclipse version 11.31 with IMRT to an aspherical target volume greater than 100 cc. Patient plans with breast cancer were not used, as collimator rotation is routinely implemented. Small tumors were also not considered due to the associated small jaw sizes that have minimal differences with collimator angles. Spherical lesions were dismissed due to symmetry and non-unique solutions. All patient plans used Varian IX, TrueBeam, and Trilogy accelerators with an anisotropic analytical algorithm (AAA) for dose modeling.

An example of a pelvic, lung, and head and neck case can be seen in Figures 13, 14 and 15, respectively. Pelvic patient cases consisted primarily of cancers afflicting the prostate, seminal vesicles, and lymph nodes, with margins of approximately 1 cm to create the PTV. Other pelvic patient cases consisted of rectal, bladder, and cervical cancers with similar margins around the GTV that were determined by a radiation oncologist.

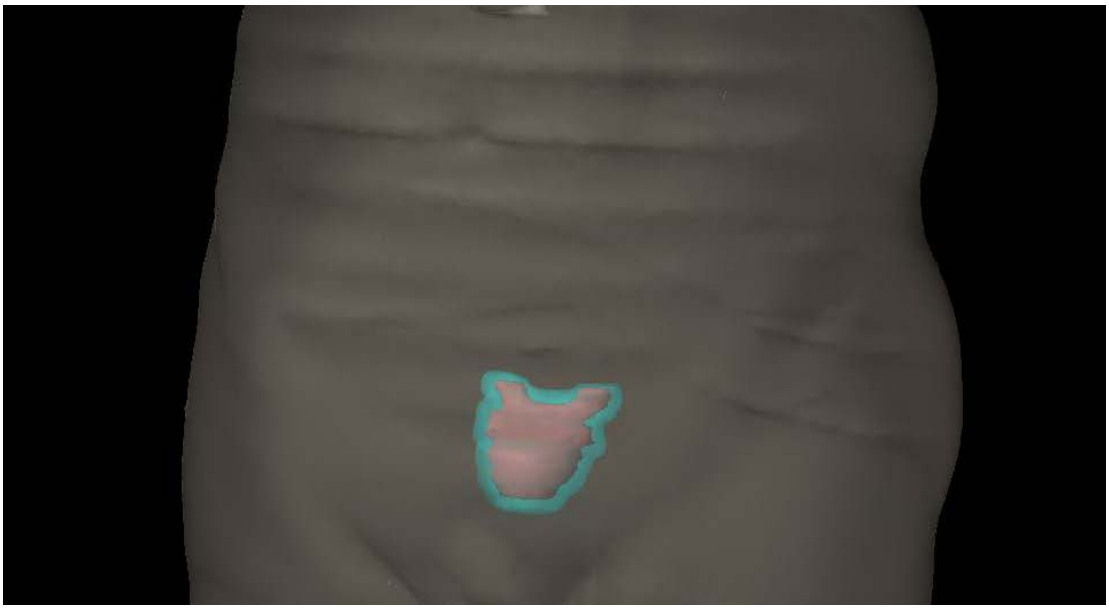

Figure 14: A pelvic cancer patient's GTV is shown in red including margins for the PTV shown in blue. The PTV is the target for radiation to be covered by the prescription dose.

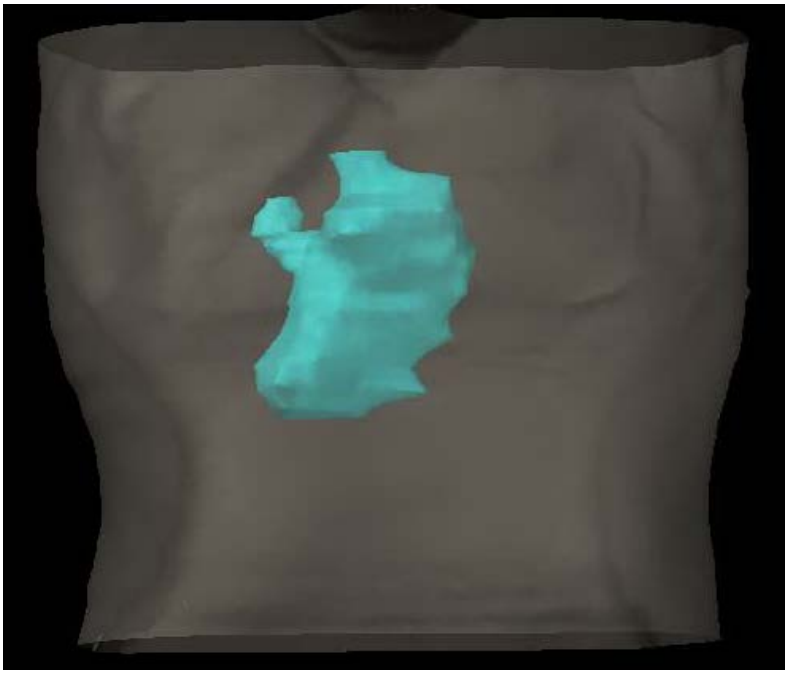

Figure 15: The PTV of a lung patient. IMRT is used to shape the dose to the asymmetric target volume.

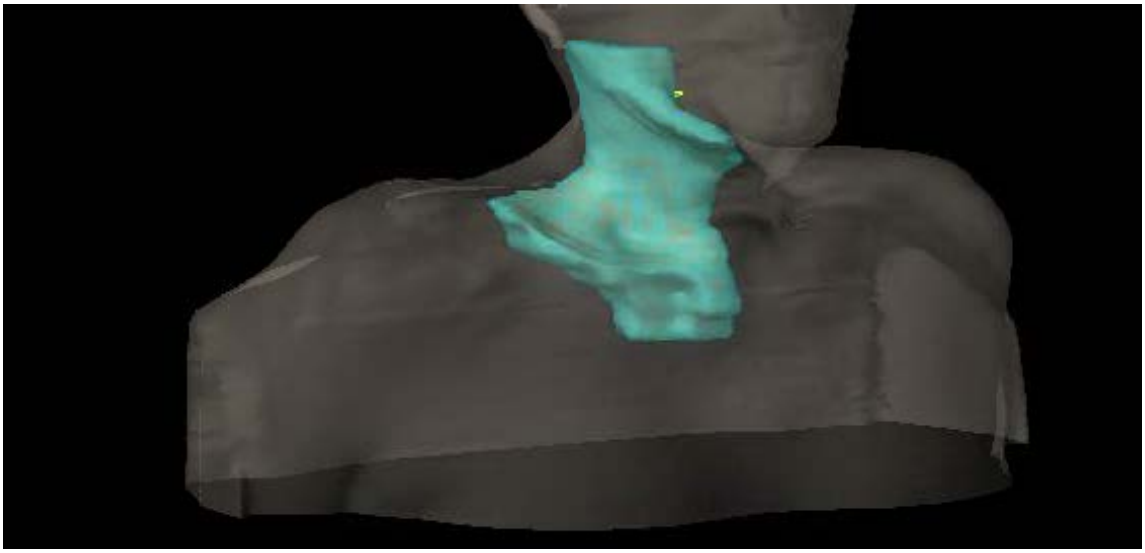

Figure 16: A lateral head and neck patient's PTV is shown in blue. The organs at risk include the spinal cord, parotids, and esophagus.

2.2 Collimator Optimization CA_A and CA_X

To determine the collimator optimization, an image of the PTV was taken in the beams eye view (BEV) for each gantry angle of the plan as in Figure 16. The image is then run through the custom macro script in *Java* and run with *ImageJ*:

```
open("C:\Image.png");
for (i=0; i<180; i+=1) {
    run("Smooth");
    run("8-bit");
    run("Arbitrarily...", "interpolate enlarge angle="+i);
setThreshold(30, 200);
    run("Set Measurements...", "bounding redirect=None decimal=3");
    run("Analyze Particles...", "display");
    run("Revert");
}
close();
```

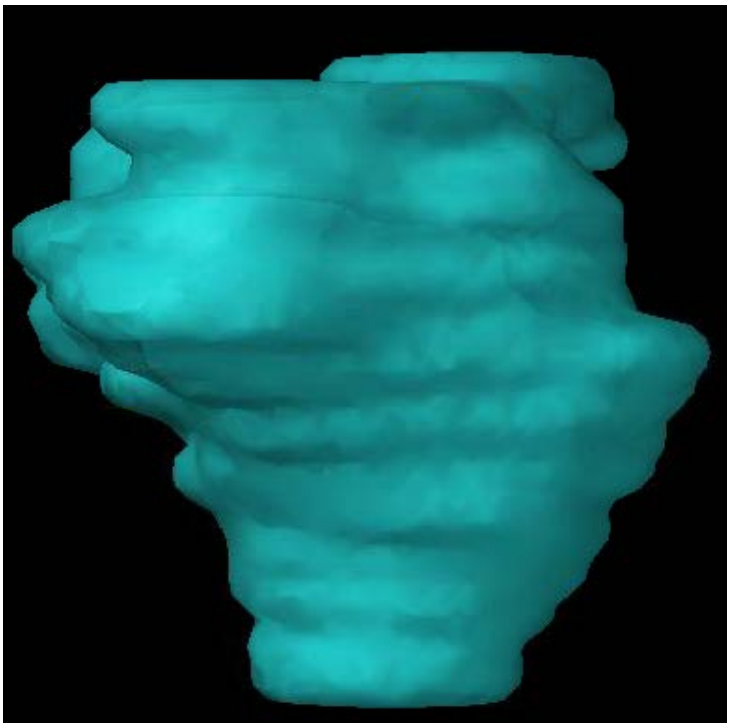

Figure 17: : The image capture of the PTV of the beam's eye view of a field. The image is analyzed in *ImageJ* using a custom script to find the collimator angles for CA_A and CA_X.

The images are sent to a directory where the script analyzes each PTV file in *ImageJ*. The images are first converted to 8-bit and a threshold was set between 30 and 200 to distinguish the PTV image from the background as is shown in Figure 17.

Figure 18: A script for CA_A and CA_X converts the image of the PTV to 8-bit color scheme to distinguish the edge of the PTV. A threshold is applied to render the image into a continuous body to be analyzed.

A bounding box then finds and records the width and height of the box that would circumscribe the PTV. The image is rotated at intervals of 1º and the process is repeated for 179 more iterations. The data from the height and width of the bounding box is then transferred to a spreadsheet. For the CA_A collimator angle, the angle that is used are chosen as the minimum value for the product of the height and width. Similarly, the minimum value of the width of the box is recorded for the angle used in the CA_X method. The angles are divided between 0º and 89º and 270º-359º to avoid the symmetry solutions and to keep the collimator from turning past limitations. Figure 18 shows an example of the x-jaw field size with respect to the collimator angle. The angle used for the CA_X from this information is 323º. The same process for CA_A gives a collimator angle of 351º.

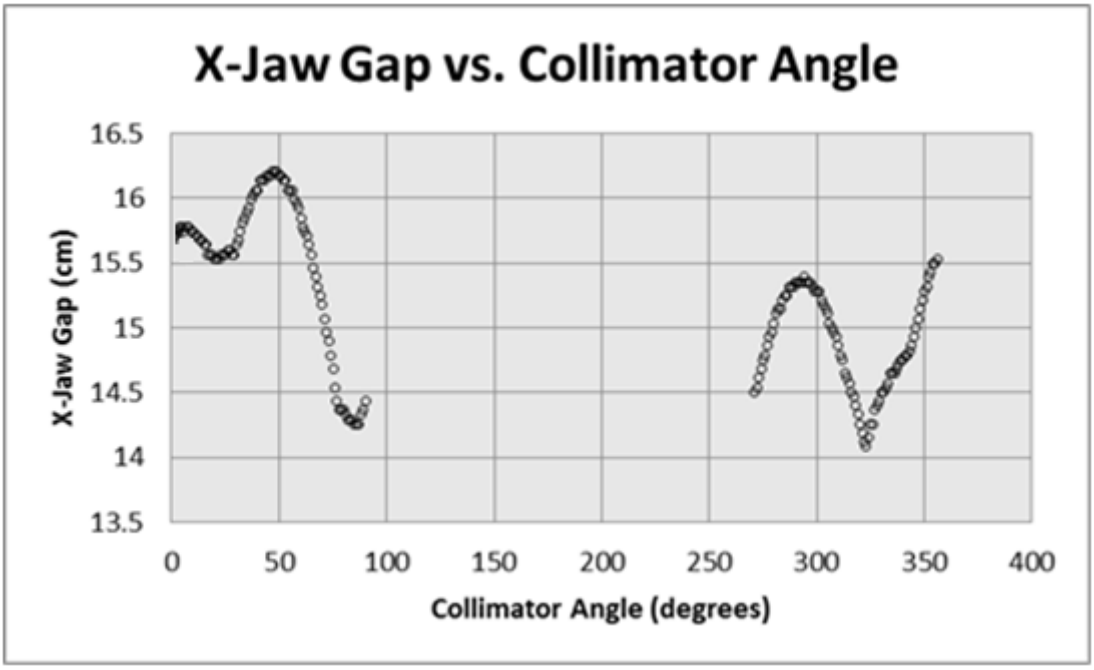

Figure 19: The x-jaw gap is plotted from the data of the bounding box in *ImageJ*. The global minimum of the graph is picked out automatically and stored as the angle to be used for CA_X. A similar process is used to find the collimator angle for CA_A.

The results of the CA_A and CA_X are shown in Figure 19 with the box that coincides with the position of the jaws in the treatment plan.

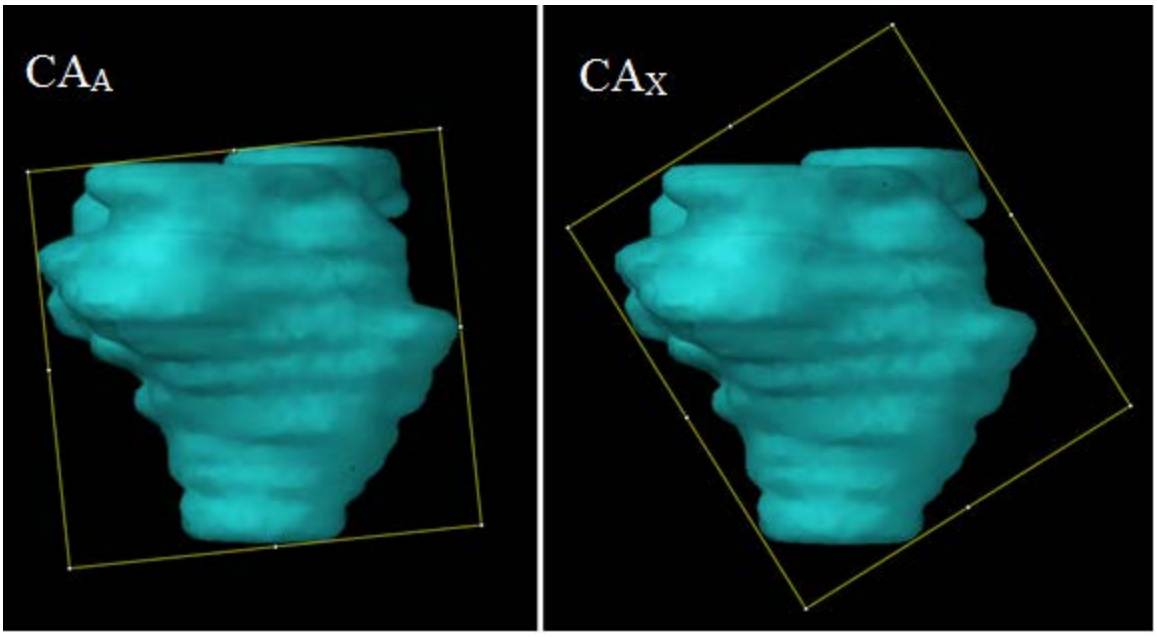

Figure 20: The circumscribed box in *ImageJ* for the respective CA_A and CA_X optimization methods. The collimator angle is then used in the Eclipse treatment planning software.

The information for each field is entered into Eclipse before the optimization. For the Eclipse optimization, each field is assigned the PTV as the target volume and the collimator is chosen by Eclipse. For the CA_0, all fields are set to an angle of 0º. The setup of the four different angles is shown in Figure 20. It should be noted that the CA_A field split and only shows the jaw position of the first segment of the field.

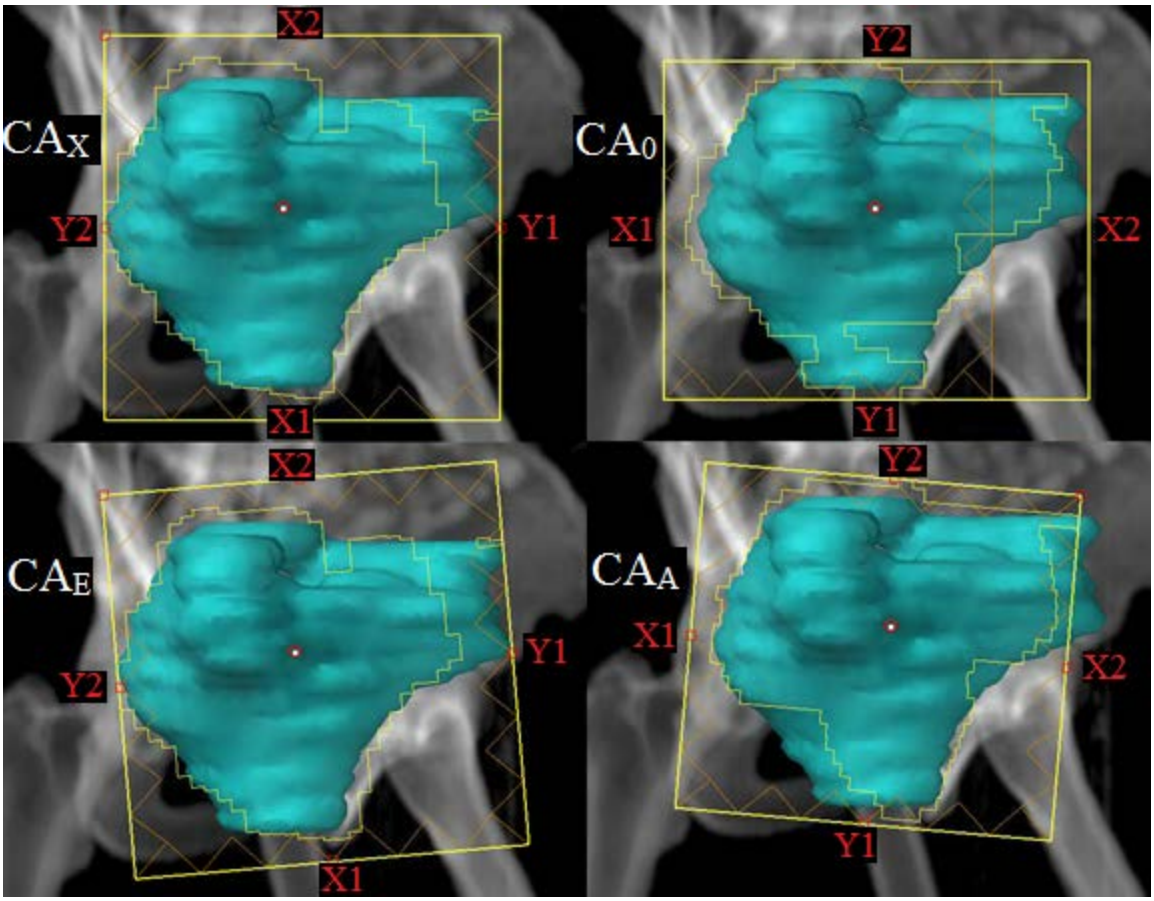

Figure 21: A depiction of the four optimizations for a single field. The MLC leaves are outlined on the inside of the box and the solid yellow lines represent the jaw positions. The MLC leaves move in the direction from X1 to X2. The field for the CA_A optimization split as leaves were required to travel more than 14.5 cm. In this case, only the first subfield is shown.

2.3 Planning

The plans were originally created by a group of highly trained dosimetrists and replanned with the original constraints. There was no fluence editing done at the end of optimization to eliminate any human influenced differences that could cause bias in the plans. Once the dose optimization was achieved, the plans were renormalized to the original planned values. The fraction dose for all plans was set to 180 cGy to avoid one plan requiring significantly more monitor units for evaluation. The dose distribution is independent of the fraction dose and scalable with normalizations and prescription dose.

Figure 21 shows an example of a head and neck plan that has been normalized from the PTV receiving 100% of the prescription dose to 95% of the volume ($V_{100\%}$=95%). Figure 22 shows the same plan with a normalization value of $V_{100\%}$=100%. Overlaying the plans will show the two have only a difference in the dose scale. Consequently, the monitor units will also scale with the plan.

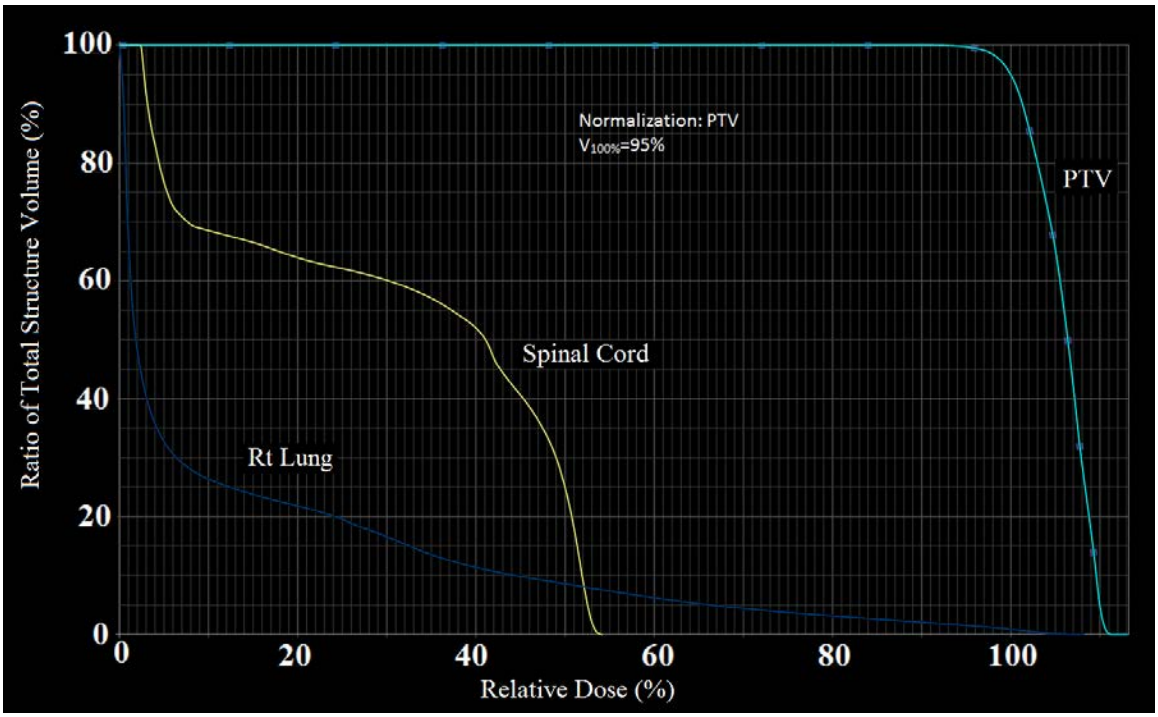

Figure 22: The dose-volume histogram (DVH) for a normalization method that forces the 100% isodose volume to cover 95% of the PTV. Normalizing is often used to scale an optimized plan to meet criteria to add tumor control or reduce tissue complication.

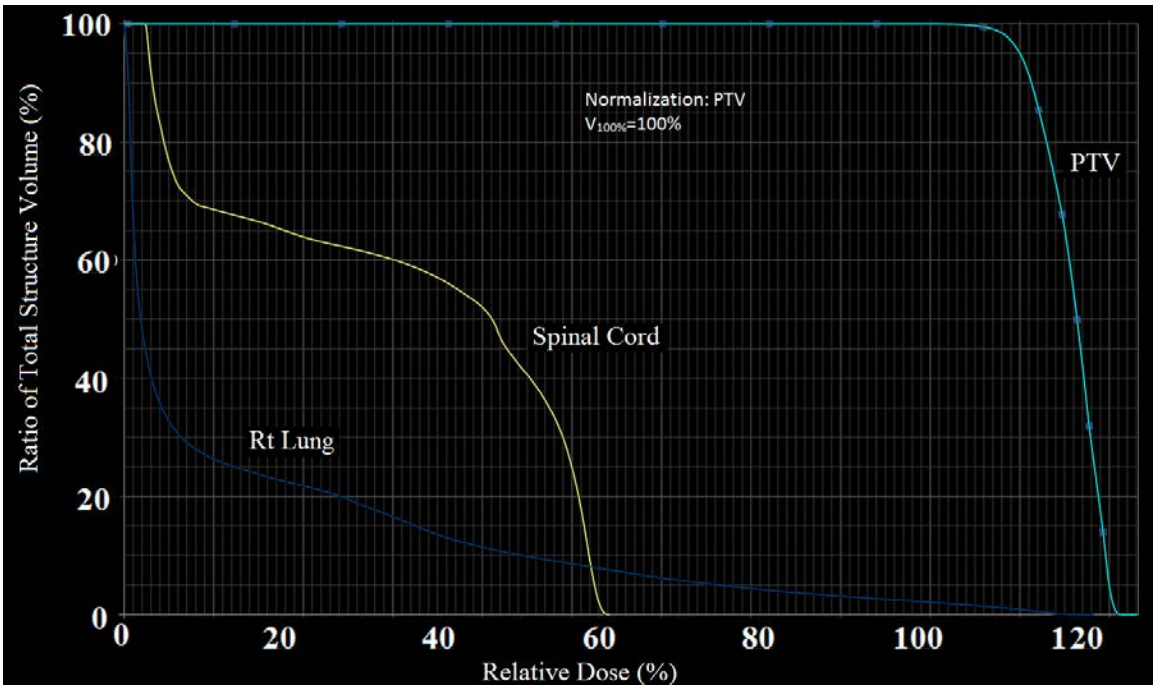

Figure 23: The same DVH as in Figure 21 with a different normalization. The dose distribution stays the same but the scale changes. The same effect occurs when the prescription dose changes. For plan evaluations, all plans were set to the same fraction dose of 180 cGy.

3. RESULTS AND DISCUSSION

3.1 Data Metrics

The data collected were analyzed statistically for six metrics: the number of monitor units each plan used, the maximum dose in the body, the maximum dose to the nearest two organs at risk which was determined per plan, the number of fields that split, and the conformity index. Plan dose distributions were evaluated qualitatively with dose volume histograms and fluence modeling. The plan delivery was analyzed with a portal dosimetry for quality assurance.

3.2 Monitor Units

The monitor units of the plans were evaluated for each case after the plan was optimized, normalized to the same value as the original plan, and set to a fraction dose of 180 cGy. The dose rate used for all plans was set to 600 MU/min. The average number of monitor units for the CA_0 plans was 1,376, which was the second highest of the four optimizations. Using the Eclipse optimizer to choose the collimator angle for CA_E dropped the number of MU by about 2% to 1,350. Minimizing the area of the jaws had the highest MU count at 1385, which was an increase of about 1%. The lowest MU was from the CA_X plans, which dropped the MU by 6% from the CA_0 to 1293.

Lowering the number of monitor units is beneficial to both patient delivery and patient safety. Lowering the monitor units reduces the amount of leaked radiation through the head of the gantry. The excess leakage radiates the entire body of the patient and can cause secondary cancers[46]. Lowering the amount of monitor units the treatment requires

also reduces the amount of time that a patient needs to be on the table during the delivery process. Limiting the amount of delivery time reduces the amount of patient motion during radiation. Lowering the monitor units also lowers the modulation of the plan. While modulating a plan is the intent of IMRT, over modulating can increase the planned and delivered distribution differences.

3.3 Maximum Dose to the Body

The maximum dose to the body or the plan is used when evaluating a plan for treatment. The maximum dose is generally located inside the PTV and best if located inside the GTV. Distributions that are outside of these conditions generally result from a poor choice of constraints during the optimization. A maximum dose outside of the PTV gives higher normal tissue complication probabilities. All 20 of the plans tested for each of the four collimator optimizations had the maximum dose located inside of the PTV. An example of a pelvic plan is shown in Figure 30 that has a maximum dose of 110% inside of the PTV (shaded blue). A lower maximum dose is advantageous in conventional fractionation and helps with creating a homogenous dose distribution throughout the PTV.

Figure 24: The maximum dose of 110% of the prescription is located inside of the PTV (shaded blue) for a pelvic plan. Controlling the maximum dose can improve the homogeneous distribution of dose throughout the PTV.

All of the planning methods averaged a maximum dose within 1% of each other. Fluence editing is often used after optimization to reduce the maximum dose which was not provided for these evaluations to minimize a human bias in the plans. The highest maximum dose was from the CA_A method, which produced an average maximum dose of 110.31%. The next highest was from the CA_E method, which produced an average maximum dose of 110.26%. Measurements from the CA_0 plans created an average maximum dose to the body of 110.09%. The lowest average maximum dose for the treatment plans was from the CA_X plans, with an average of 109.83%.

3.4 Maximum Dose to the Organs at Risk

The maximum dose to the organs at risk (OAR) is important when assessing the safety and quality of a plan. While radiation therapy can be effective in giving lethal doses to tumor volumes, the organs around the target will always receive some

percentage of radiation. *Serial* organs will only remain functional if the entire organ survives, making it crucial that the entire structure remains under thresholds determined from radiation oncologists.

For the ten pelvic patient cases, the most at risk organs for the plans included the rectum and the bladder. If the PTV was inside the structure, only the volume that was outside of the PTV was evaluated. Contours were determined from experienced dosimetrists and contours for the PTV were outlined from the radiation oncologist. In the five head and neck patient cases evaluated, the most at risk organs were the spinal cord, parotids, esophagus, trachea and mandible. The five lung patient cases included the contralateral and ipsilateral lungs, spinal cord, heart, trachea, esophagus, carina and liver OARs. The two organs most at risk, OAR_1 and OAR_2, were evaluated for each plan for all studied patient cases.

The CA_0 method of collimator optimization controlled the average maximum dose for OAR_1 and OAR_2 to 103.47% and 101.48% of the prescription dose. Using the *Eclipse* optimizer CA_E was slightly higher for each organ at 103.49% and 102.20% for OAR_1 and OAR_2, respectively. The best results for both OAR_1 and OAR_2 came from the CA_A method, which reduced the OAR_1 to 102.42% and OAR_2 to 101.13%. Reducing the amount of area the jaws have exposed limits the amount of radiation from leaf leakage that would be expected and could account for the drop in maximum dose. The plans for CA_X did nearly as well, reducing the maximum dose to OAR_1 to 102.94% and OAR_2 to 101.22%.

3.4.1 Organs at Risk Evaluated with a Dose Volume Histogram

Many organs are *parallel* and are better evaluated with a dose volume histogram (DVH) since the organ can still function even if a portion of it becomes necrotic. The

qualitative analysis showed a decrease in dose for organs at risk with the new CA_X method of optimization from the CA_0 plans. This drop can be seen with the lower isodose volumes, even if the maximum dose remains close to the same. A conventional fractionation dose constraint for several organs is given in Table 1 from Radiation Oncology Therapy Group RTOG reports.

Conventional Fractionation			
Structure Name	Type	Volume	Dose
Bladder	Volume (%)	15%	<80 Gy
Bladder	Volume (%)	25%	<75 Gy
Bladder	Volume (%)	35%	<70 Gy
Bladder	Volume (%)	50%	<65 Gy
Femoral heads	Max Dose	None	<50 Gy
Femoral heads	Volume (%)	25%	<45 Gy
Femoral heads	Volume (%)	40%	<40 Gy
Penile bulb	Mean Dose	None	<52.5 Gy
Rectum	Volume (%)	15%	<75 Gy
Rectum	Volume (%)	25%	<70 Gy
Rectum	Volume (%)	35%	<65 Gy
Rectum	Volume (%)	50%	<60 Gy
Spinal cord	Max Dose	None	<45 Gy

Table 1: Dose constraints with conventional fractionation for some pelvic organs at risk from the Radiation Oncology Therapy Group (RTOG) reports.

Inspection of a DVH of the CA_X plans compared to the CA_0 method showed decrease in the lower dose regions of the organs at risk. As the example for a lung patient

case in Figure 24 shows, the dose to the carina, spinal cord, and trachea were all controlled better by the CA_X plan (triangles) from the CA_0 method (squares) in the lower relative dose regions while maintaining only minor differences in the tumor control.

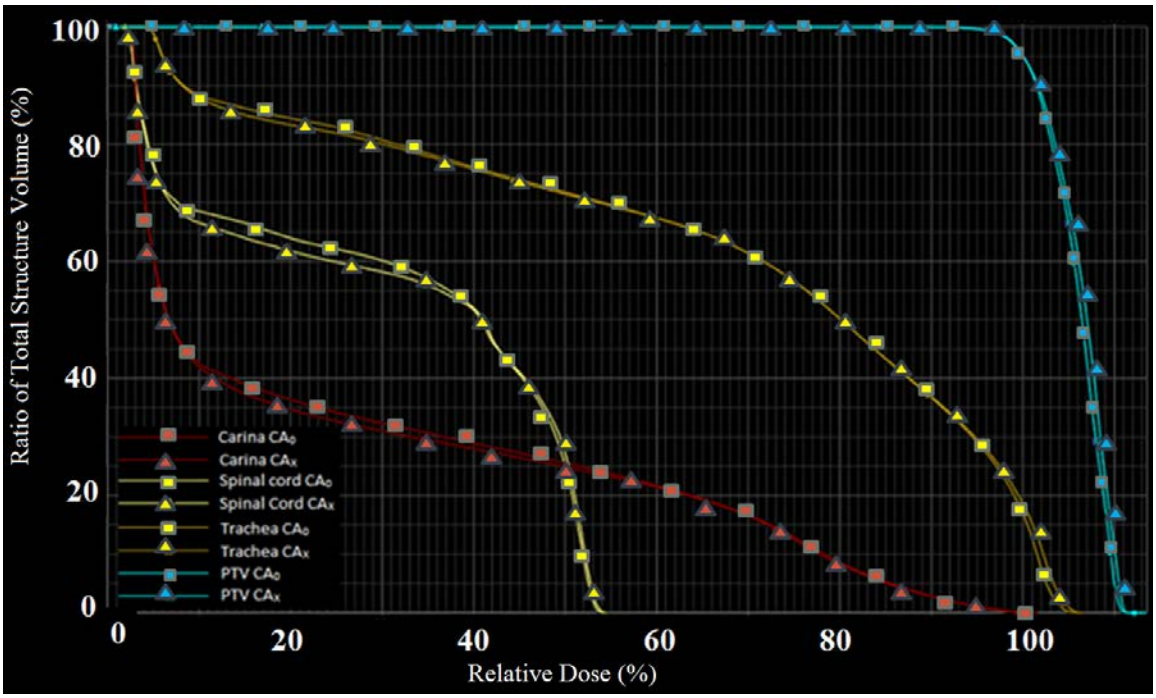

Figure 25: A DVH showing the differences between the CA_0 (squares) and CA_X methods of optimization for a lung patient case. The lower radiation levels for the carina, spinal cord, and trachea was achieved by the CA_X planning method for relative dose values between 10% and 30%.

3.5 Conformity Index

The conformity index (CI) of a plan is used as one tool to quantify the tumor control by calculating the ratio of the 100% isodose volume to the PTV volume. A ratio over one will always indicate that normal tissue is being irradiated by the prescription dose value while a ratio under one shows underdosing to parts of the PTV. Values close to one are desirable; although a perfect ratio will show equal volumes, it lacks the spatial information that would give matching locations. The Paddick Conformity Index corrects for the coordinates of the isodose distribution and the target.

All of the CI ratios were found to have negligible difference. The average CI varied insignificantly from each method on the individual plans as well as the total average of all the measurements. The average CI value for the CA_0, CA_E, CA_A and CA_X plans were 1.039, 1.045, 1.037, and 1.040 respectively. This indicates that all methods throughout the study gave comparable tumor control.

3.6 Monitor Units

The monitor units (MU) of a plan determine the current that the linear accelerator delivers through the gantry. This stream of electrons is then directed onto a target where the kinetic energy of incident electrons is converted to photons. The dose rate and the amount of monitor units determine the time that a field will take to deliver. A dose rate of 600 MU/min was applied to all of the treatment plans.

The CA_0 method of delivery averaged a total of 1,376 monitor units that were used to deliver one fraction of the treatment. The Eclipse collimator optimization, CA_E, lowered the average MU slightly to 1,350 from the CA_0, while the CA_A method increased to 1,385 MU. By reducing the modulation with the CA_X plans, the average monitor units dropped significantly by 6% from the CA_0 plans to 1,293. This drop in MU can increase the efficiency of treatment delivery and lower the amount of time that a patient is on the table. It also decreases the amount of radiation that is leaked through the head of the gantry, which has a linear relationship to the amount of MU being delivered.

The monitor units being delivered were the lowest for CA_X in 11 of the 20 patient plans tested. The average MU for the CA_X method remained close to 6% less than CA_0 in each tested region of pelvic, lung, and head and neck. Assuming an average patient load of 40 patients per day, five days per week, and operating at a dose rate of 600 MU/min, a 6% drop in MU would equate to a reduction of time the machine in the “beam

on” position of about 26 minutes per week. This not only impacts the safety of the patient but also reduces the radiation to the therapists and staff near the vault.

3.7 Split Fields

A field will split when the multileaf collimator (MLC) moves more than 14.5cm across the x-jaw gap, producing two subfields that are loaded individually. Each field was measured to take about 15 seconds for a therapist to load during treatment delivery. This time accounts for both the shift of the x-jaws and MLC to move into a new placement as well as a new calibration check that a machine runs automatically for a new field when loaded for delivery. Split fields have the disadvantage of having to match the dose line from the previous subfield and are prone to errors proportional to the dose gradient of the penumbra.

The total number of split fields produced by all 20 plans for the CA_0 method was 61. Optimization with the Eclipse collimator option increased the number of split fields to 63, the highest among the tested methods. Using CA_A did marginally better with a total split field difference of 60. Minimizing the x-jaw gap, which should give the lowest results theoretically, dropped the amount of split fields by over 38% to a total of 37. This reduction in split fields is attributed to minimization of the amount of distance that the MLC must move, which is directly related to whether a field will split or not. In one patient case that was tested, all nine fields split for each of the three other methods, while the CA_X method resulted in no split fields. In total, ten cases resulted in split fields for at least one method. Of those ten, three were reduced to no split fields by using a CA_X approach. Only in three cases was the CA_X method unable to find a way to reduce the number of split fields from the other methods.

Minimizing the number of split fields would be a significant improvement in several instances for planning. Not only would it save time for patient delivery and quality assurance (QA) testing, it could also reduce the errors that occur with subfield match lines due to patient movement. Even a small amount of motion from a patient can lead to a gap in the radiation treatment delivery because the radiation is no longer being delivered continuously when using a sliding window for MLC modulation.

Based on the information gathered for a treatment of 40 patients in a week with a similar set of patient plans, it is estimated that the time that a therapist would save by reducing the number of split fields would be about four minutes per week in loading extra subfields.

The QA of plans is often evaluated per field by a physicist before being approved for treatment delivery. A nine-field plan that has split will take considerably longer to evaluate with a diode array such as a MapCheck. Additionally, the fields have been observed to have a lower pass-rate when a sub-field has a small amount of monitor units.

3.8 Summary of Results

The averaged results of all the metrics tested with the four methods showed that the CA_X method leads to improvement in MU, and split fields as demonstrated in Table 2. The other three metrics were improved, although insignificantly, by minimizing the area of the jaws, which showed a lower average maximum dose to the two most at risk organs per plan as well as a slightly improved CI value. The results are summarized in Table 2.

Metrics Summary				
	CA_0	CA_E	CA_A	CA_X
Avg. MU	1376	1350	1385	1293
Avg. Plan Max Dose	110.09%	110.26%	110.31%	109.83%
Avg Max to OAR_1	103.47%	103.49%	102.42%	102.94%
Avg Max to OAR_2	101.48%	102.20%	101.13%	101.22%
Avg CI	1.039	1.045	1.037	1.040
Total Split Fields	61	63	60	37

Table 2: A summary of the six measured metrics. The CA_X produced the lowested MU and number of split fields.

Figure 25 shows each metric normalized to the CA_0 method of collimator rotation. Since much of IMRT planning is done with collimator angles kept at 0º for all fields, it is reasonable to use the CA_0 as the standard to compare different planning methods. The drop in MU can be seen from the CA_E and CA_X methods of collimator optimization. A slight decrease in the maximum dose is also shown for the maximum dose to the body for CA_X. A decrease in the maximum dose to the OAR_1 and OAR_2 was observed with the CA_A and CA_X methods as well, while an increase the CA_E method gave a small increase to the second organ at risk. The CI values all remained similar, indicating that the tumor control stayed relatively independent of the collimator optimization. The split fields showed a dramatic decrease with the CA_X method by minimizing the distance that the leaves must travel for each individual field.

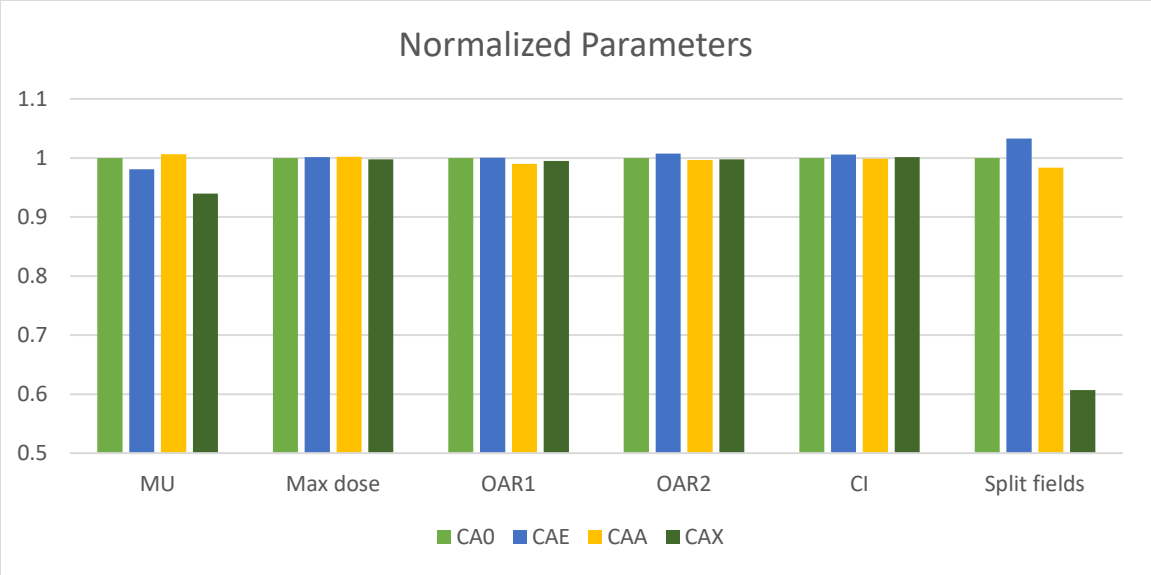

Figure 26: A plot of the averaged results with each metric normalized to a value of 1 for the CA_0 collimator optimization method. The CA_X was close to equal or better in all metrics tested. The CA_A made slight improvements in the average maximum dose to the organs at risk. The Eclipse collimator optimizer made a small improvement in monitor units to the CA_0 while creating more split fields and insignificant changes in the maximum dose to the organs at risk. The lowered split fields for the CA_X method was that most drastic change observed.

3.9 Statistical Evaluation

A one way analysis of variance (ANOVA) was evaluated, comparing each method to another for every metric. The results of the statistical testing p-values are summarized in Table 3. The Table highlights p-values less than or equal to 0.05.

One way ANOVA p-value						
	CA_0 vs CA_E	CA_0 vs CA_A	CA_0 vs CA_X	CA_E vs CA_X	CA_E vs CA_A	CA_A vs CA_X
Monitor Units (MU)	0.20	0.67	0.01	0.31	0.27	0.05
Maximum Dose	0.32	0.49	0.56	0.92	0.42	0.37
Max to OAR_1	0.99	0.79	0.89	0.89	0.78	0.89
Max to OAR_2	0.87	0.94	0.96	0.81	0.81	0.79
Conformity Index	0.88	0.97	0.97	0.91	0.84	0.94
Split Fields	0.26	1.00	0.02	0.01	0.84	0.02

Table 3: A one way ANOVA Table showing the p-values of the four collimator methods for each metric. The highlighted results show significant decrease in the monitor units for the CA_X collimator method versus keeping the collimator at 0º and minimizing the area of the jaws. There is also a substantial decrease in split fields with CA_X compared to all other methods tested.

The Table highlights the significance of the CA_X collimator optimization for monitor units against the standard CA_0 planning technique. The drop in MU for the CA_X collimator optimization was significant compared to CA_0 and CA_A. There was also a strong statistical significance in decreasing the number of split fields using CA_X compared to the other tested methods of collimator rotation.

3.10 Fluence Modeling

After the dose optimization, a fluence pattern was generated, which calculates where the leaves of the MLC must move in order to generate the desired dose pattern. A gradient in fluence is what gives IMRT the power to shape the dose patterns by calculating the fluence for each bixel. The resulting fluence distributions from each field will generate the voxel dose. Figure 26 shows the fluence patterns generated from the same field for each method of optimization. The high gradient areas indicate where the leaves in the collimator heavily modulate the fluence.

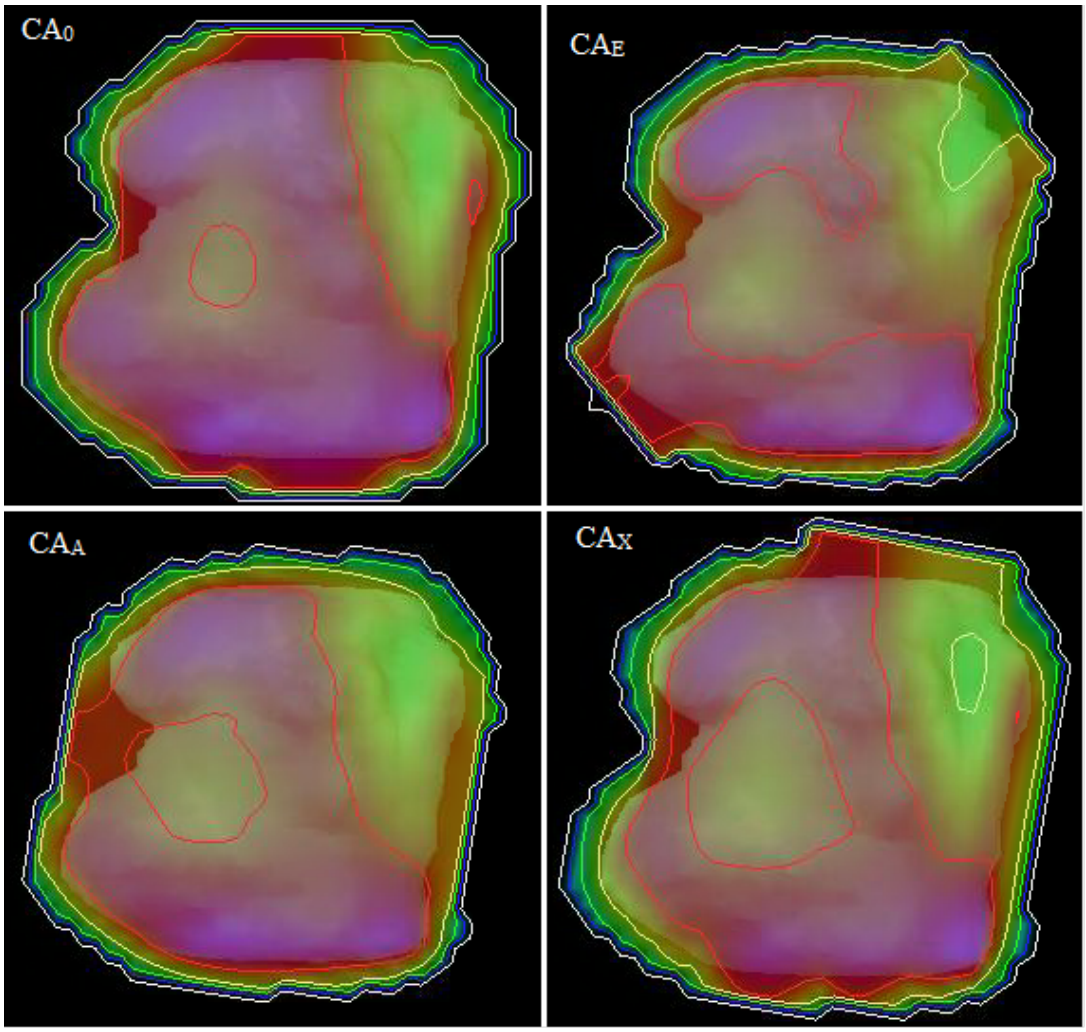

Figure 27: The fluence generated for a single field from each of the four methods. Changing the collimator angle will change the bixel map that is used in Eclipse to generate the leave motion.

3.11 Plan Quality Assurance

There are several systems that are used to measure the quality of a plan before a patient is treated. In this research, an electronic portal imaging device (EPID) was used to verify the plans created with each technique and delivered each field to be analyzed. The results of the tests can show the predicted values to compare with those that were delivered onto the EPID. In the testing of a field shown in Figure 27, the red indicates areas where the predicted and the delivered radiation were outside of a 2%, 2mm gamma

tolerance using a 10% threshold. The threshold is the percentage from the maximum that is neglected from the comparison. This will exclude the lower values from the calculation.

The pass rate for this particular field was 94.0% for the CA_0 optimization. The CA_X and CA_A improved this to 95.9% and 96.0%. The highest improvement was found from the CA_E, with a pass rate of 97.4%. While the result for a single field does not qualify as statistically significant, it demonstrates that the quality of a plan can be influenced by the collimator. The tolerance was chosen to demonstrate the differences between the planning techniques.

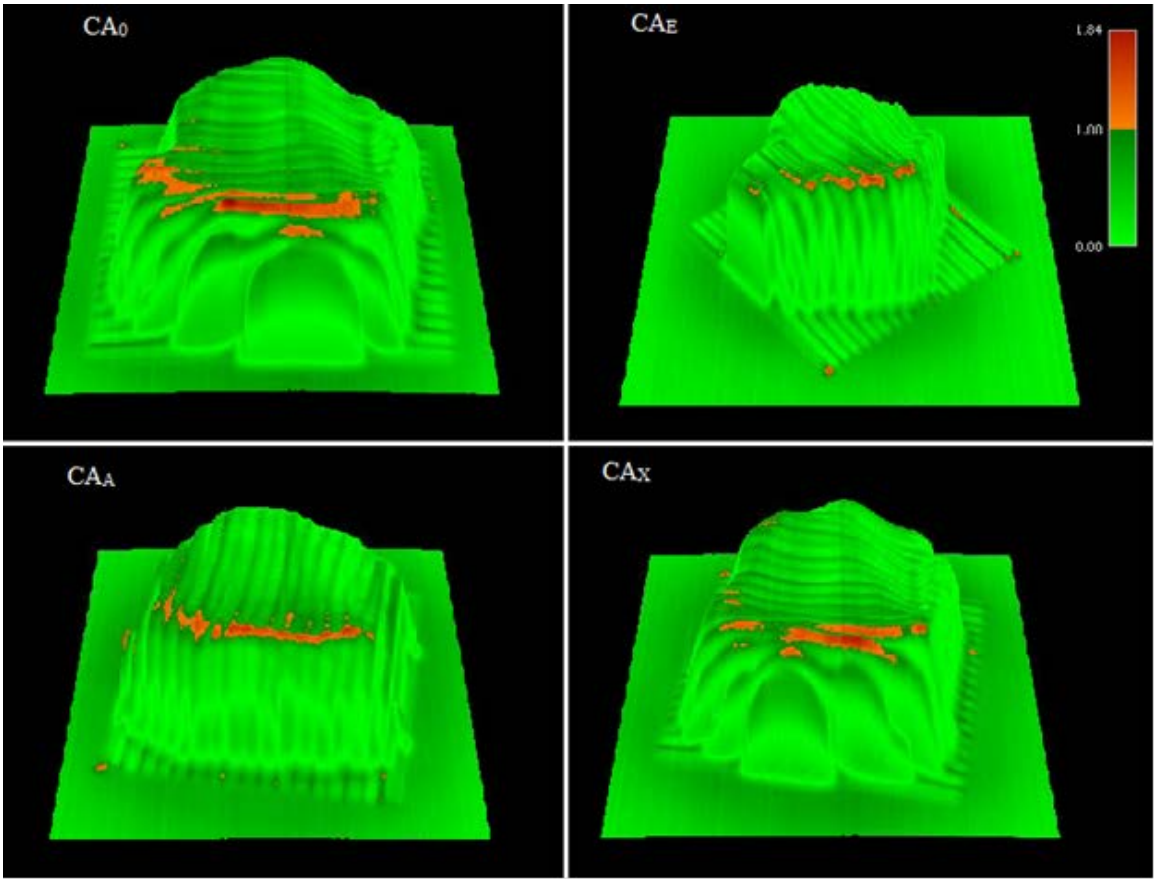

Figure 28: Portal dosimetry for a field delivered with the four collimator methods. The red portions indicate a failed gamma with a tolerance of 2% and 2 mm of the predicted value.

An advantage for allowing the collimator to be rotated can also be shown with the interleaf leakage. For a collimator to remain at 0º for each field, each leaf will remain in a single plane independent of the gantry position. The interleaf leakage has been measured to be about 2% of the open field dose. Due to this leakage, the differences between predicted outcomes can sum to produce noticeable deviations from a delivered plan. It is noted that a single value for the interleaf leakage is supplied in the planning system, while the individual values between different leaves may vary. A nine field plan was delivered with a CA_0 approach and a CA_X optimization shown in Figure 28. The jagged edges of the CA_0 delivered plan are caused mostly from the interleaf leakage. The same plan was delivered with the CA_X method of optimization and allowed to rotate with the delivery of the composite of all nine fields. The results show a distribution of dose that is smooth and better matches the outline of the predicted fields.

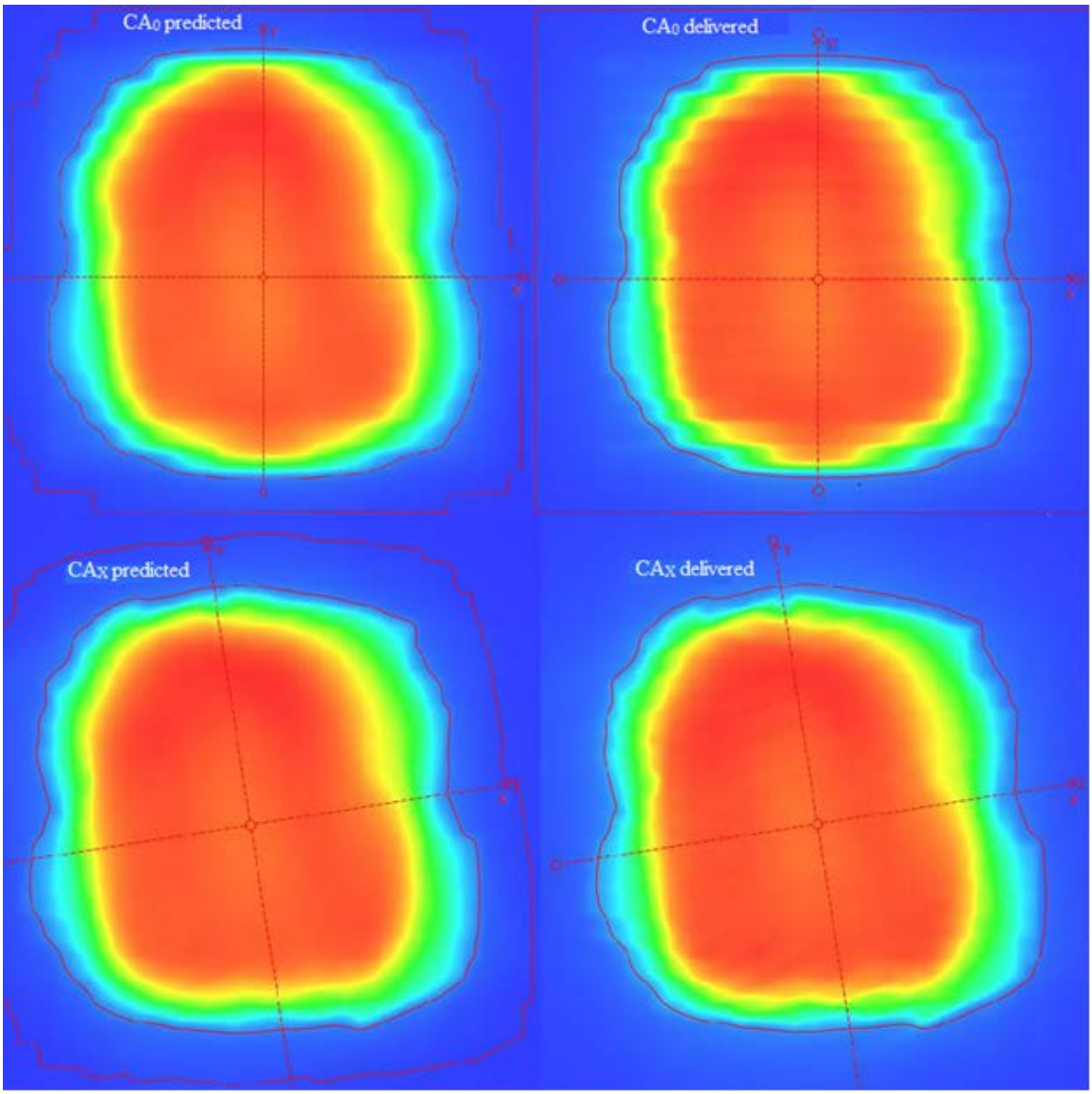

Figure 29: A predicted dose distrubution for the CA_0 and CA_X, left, compared to a composite dose delivered on an electronic portal imaging device (EPID), right. By rotating the collimator, the error associated with the interleaf leakage is averaged out and forms a smooth dose distrubution.

The portal dosimetry can be viewed on the axes of the graph to depict the severity of the deviations in the profile. In Figure 29, the green line shows the corresponding delivered dose along the y-axis for the CA_0 and CA_X plans. The green line oscillates between the predicted calibrated units (CU) values due to the single value that is allowed for the leaf transmission factor. The oscillations become more evident for the thicker leaves, which

are located away from the center of the field. In the CA_X plan, these oscillations are smoothed out by rotating the collimator between fields.

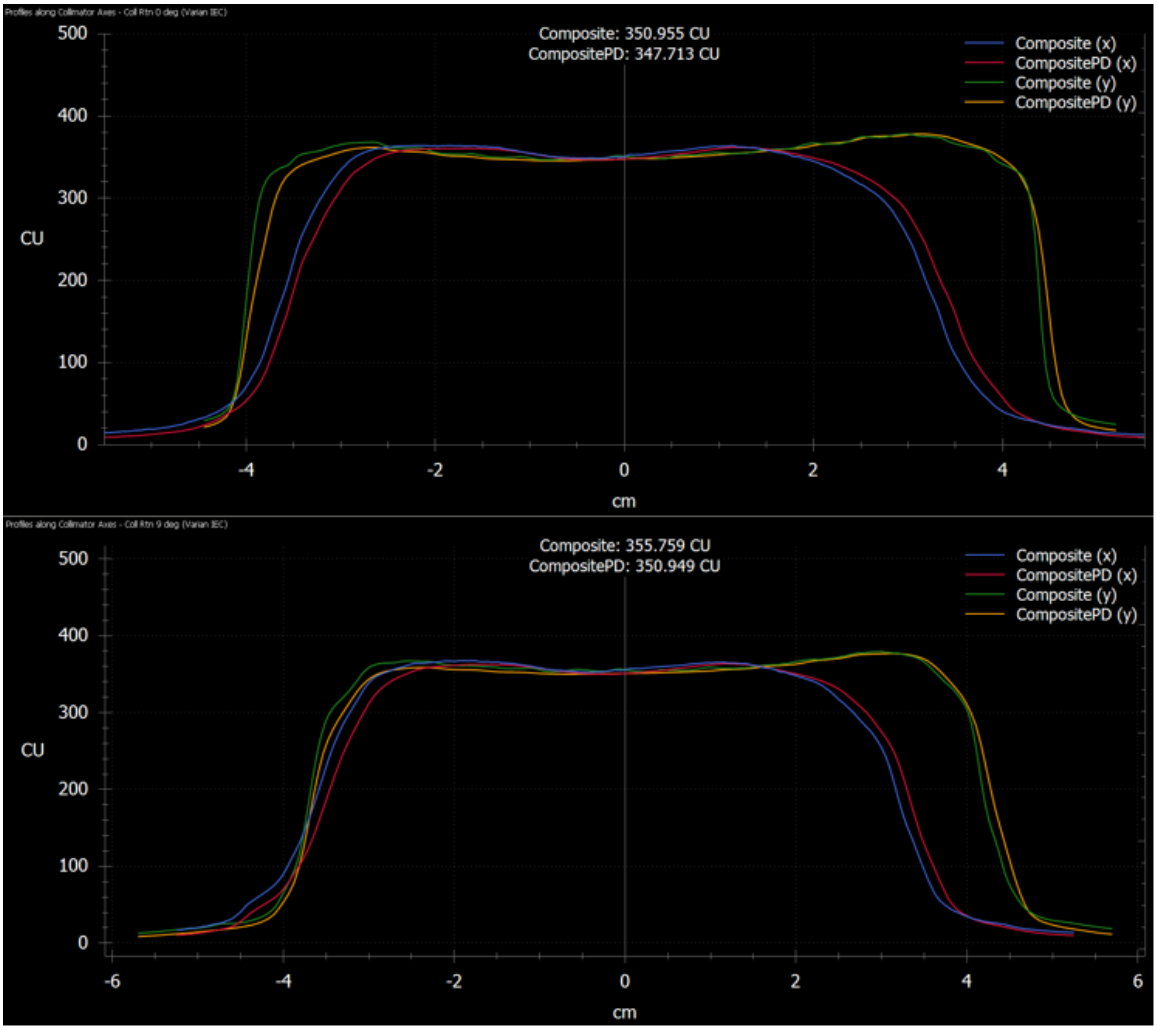

Figure 30: The axes of the portal dosimetry showing the expected (compositePD) and delivered (composite) calibrated units (CU) for the CA_0 composite (top) and CA_X composite (bottom). The green, delivered curve shows fluctuations from the interleaf leakage in CA_0 whereas it is smoothed out in plans created with CA_X (bottom).

Another view of the portal dosimetry fields is shown in Figure 30 with the predicted values as dashed lines and delivered values as solid lines. The jagged edges of the delivered curve show where the algorithm deviates from the true values of which are

delivered. Applying rotations in the collimator better predicts the shape of the dose distribution.

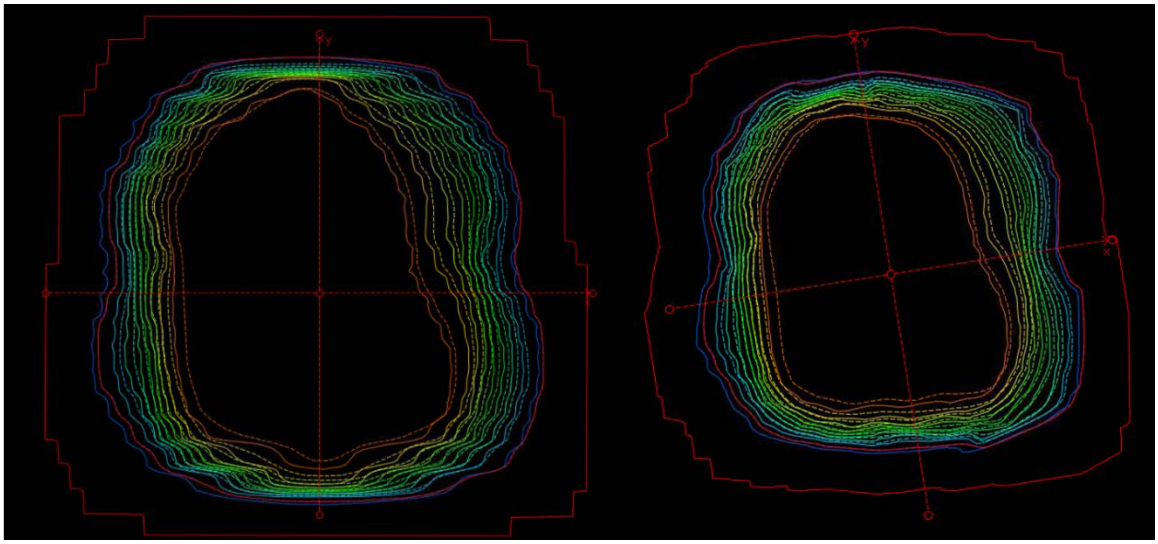

Figure 31: The predicted (dashed) and delivered (solid) dose patterns for an EPID. The jagged edges of the delivered pattern in CA_0 (left) are smoothed out by rotating the collimator between fields with CA_X (right).

4. CONCLUSION

For aspherical lesions larger than 100 cc, rotating the collimator to minimize the x-jaw gap produced equal tumor control while reducing the toxicity to the organs at risk, lowering the monitor units, and creating less split fields compared to keeping the collimator fixed at 0º (CA_0) or by using the *Eclipse* collimator optimization method (CA_E). Compared to the fixed collimator angle, the monitor units decreased on the average by 6% using a CA_X approach, which was the lowest of the four methods tested. The maximum dose to the organs at risk also showed trends of decreasing, as well as evidence of decrease of the peripheral dose as viewed with a DVH. The number of split fields was highly controlled with CA_X by optimizing the parameter that determines if a field will divide. Of the 20 cases studied, the number of split fields decreased by about 40% with the CA_X compared to any other method used.

The CA_X optimization allowed for a rotation of the collimator between each field, which showed positive results in the overall dose shape of the delivered quality assurance tests on an electronic portal imaging device. The interleaf leakage predicted for the fields cumulates to give greater deviations on the edges of the profile for a CA_0 method. It is shown that allowing the collimator to rotate alleviates the addition of errors from keeping the leaves in the same plane of gantry rotation and smooths out the final delivered result. Using the CA_X method that allows this collimator rotation has improved the shape of the final delivered dose.

None of the differences for the CA_A were tested to be statistically significant. Overall, the method that tested to give the best clinical results that resulted in more predictable outcomes for patient safety and quality assurance was with a CA_X optimizer by minimizing the x-jaw gap.

The research is limited to the scope of testing by a small subset of experienced dosimetrists. Evaluating the whole field of radiation oncology would provide a better scope of the differences that collimator optimization could make in the field of radiation oncology and medical physics. Further studies in the methods of optimizing radiation planning techniques would aid in the development of more consistent, improved quality radiation plans for treatment of cancer patients.

REFERENCES

1 Chapek, Julie, Matt Tobler, Beau J. Toy, Christopher M. Lee, and Dennis D. Leavitt. "Optimization of Collimator Parameters to Reduce Rectal Dose in Intensity modulated Prostate Treatment Planning." Medical Dosimetry 30.4 (2005): 205 12.

2 Sharma, Seema, Durai Manigandan, Shikha Goyal, and Puja Sahai. "Influence of Collimator Rotation on Dose Distribution and Delivery in Intensity Modulated Radiation Therapy for Parotid Cancer." International Journal of Cancer Therapy and Oncology 3.2 (2015): 3212.

3 "Statistics for Different Kinds of Cancer." Centers for Disease Control and Prevention. 16 Aug. 2016. https://www.cdc.gov/

4 "Comprehensive Cancer Information." National Cancer Institute. 14 Oct. 2016 https://www.cancer.gov/

5 Gabriel, Janice. "The Biology of Cancer." Chichester, England: John Wiley & Sons, 2007.

6 Egeblad, Mikala, Elizabeth S. Nakasone, and Zena Werb. "Tumors as Organs: Complex Tissues That Interface with the Entire Organism." Developmental Cell 18.6 (2010): 884-901.

7 "Cancer." World Health Organization. 23 Sept. 2016. http://www.who.int/en/

8 Leibel, S. "Technological Advances in External-beam Radiation Therapy for the Treatment of Localized Prostate Cancer." Seminars in Oncology 30.5 (2003): 596-615.

9 "Physics and Technology : Others." Radiotherapy and Oncology 88 (2008): 424.

10 "Radiation Therapy for Cancer." National Cancer Institute. https://www.cancer.gov/ 23 Sept. 2016.

11 Nilsson, Sten. "Radium-223 Therapy of Bone Metastases in Prostate Cancer." Seminars in Nuclear Medicine (2016).

12 "Cancer Facts & Figures 2016." American Cancer Society. https://www.cancer.org/ 25 Sept. 2016.

13 "The University of Chicago Medicine Comprehensive Cancer Center." What Is Cancer? 23 Sept. 2016.

14 Pennell, Nathan. "Why Lung Cancer Is the Deadliest Cancer, and Why It Doesn’t Have to Be." US News. U.S.News & World Report, 23 Oct. 2016.

15 "Lung Cancer Fact Sheet." American Lung Association. 20 Sept. 2016.

16 "Lung Cancer." American Cancer Society. https://www.cancer.org/ 23 Sept. 2016.

17 "Cancer Mortality-California Total Population." Cancer Mortality-California Total Population. 23 Sept. 2016.

18 "Lung Cancer Death Rates Fall, Helping Drive Decrease in Overall Cancer Death Rates." National Cancer Institute. 26 Sept. 2016.

19 Baskar, Rajamanickam, Kuo Ann Lee, Richard Yeo, and Kheng-Wei Yeoh. "Cancer and Radiation Therapy: Current Advances and Future Directions." International Journal of Medical Sciences 9.3 (2012): 193-99.

20 "Radiation Oncology UCLA | Back to Home." Lung Cancer Treatment.

21 Dueñas-González, Alfonso, Lesbia Rivera, Aida Mota, Carlos López-Graniel, Alberto Guadarrama, Aarón González, Gregorio Chanona, Paula Cabrera, and Jaime De La Garza. "The Advantages of Concurrent Chemoradiation After Neoadjuvant Chemotherapy for Locally Advanced Cervical Carcinoma." Archives of Medical Research 33.2 (2002): 201 02.

22 Glatstein, E., and M. Morrow. "Five-Year Outcomes After Prostatectomy or Radiotherapy for Prostate Cancer: The Prostate Cancer Outcomes Study." Yearbook of Oncology 2006 (2006): 146-49.

23 Provencio, Mariano, Dolores Isla, Antonio Sánchez, and Blanca Cantos. "Inoperable Stage III Non-small Cell Lung Cancer: Current Treatment and Role of Vinorelbine." Journal of Thoracic Disease. Pioneer Bioscience Publishing Company, Sept. 2011.

24 "Head and Neck Cancer." Radiotherapy and Oncology 83 (2007).

25 Courdi, A. "The LQ Model in the Daily Practice of Radiotherapy." Radiotherapy and Oncology 25.3 (1992): 220.

26 Williams, MV, J. Denekamp, and JF Fowler. "A Review of Alpha/beta Ratios for Experimental Tumors: Implications for Clinical Studies of Altered Fractionation." International Journal of Radiation Oncology, Biology, Physics (1985).

27 Ponsky, Lee E., and Donald B. Fuller. Robotic Radiosurgery Treating Prostate Cancer and Related Genitourinary Applications. Berlin: Springer, 2012.

28 Shrieve, Dennis C., and Jay S. Loeffler. Human Radiation Injury. Philadelphia: Wolters Kluwer Health/Lippincott Williams & Wilkins, 2011.

29 Hegemann, Nina-Sophie, Matthias Guckenberger, Claus Belka, Ute Ganswindt, Farkhad Manapov, and Minglun Li. "Hypofractionated Radiotherapy for Prostate Cancer." Radiation Oncology Radiat Oncol 9.1 (2014).

30 Hall, Eric J., and Amato J. Giaccia. Radiobiology for the Radiologist. Philadelphia: Lippincott Williams & Wilkins, 2006.

31 Radiation Biology: A Handbook for Teachers and Students. Vienna: International AtomicEnergy Agency, 2010.

32 Williams, M.v., J. Denekamp, and J.f. Fowler. "A Review of Ratios for Experimental Tumors: Implications for Clinical Studies of Altered Fractionation." International Journal of Radiation Oncology Biology Physics 11.1 (1985): 87-96.

33 Vogelius, Ivan R., and Søren M. Bentzen. "Meta-analysis of the Alpha/Beta Ratio for Prostate Cancer in the Presence of an Overall Time Factor: Bad News, Good News, or No News?" International Journal of Radiation Oncology Biology Physics 85.1 (2013): 89-94.

34 Valdagni, Riccardo, Corrado Italia, Paolo Montanaro, Angelo Lanceni, Paola Lattuada, Tiziana Magnani, Claudio Fiorino, and Alan Nahum. "Is the Alpha–beta Ratio of Prostate Cancer Really Low? A Prospective, Non-randomized Trial Comparing Standard and Hyperfractionated Conformal Radiation Therapy." Radiotherapy and Oncology 75.1.2005): 74-82.

35 Stuschke, Martin, and Howard D. Thames. "Fractionation Sensitivities and Dose control Relations of Head and Neck Carcinomas: Analysis of the Randomized Hyperfractionation Trials." Radiotherapy and Oncology 51.2 (1999): 113-21.

36 Kirova, Ym, and N. Kramkimel. "Evolution in the Management of Skin Malignant Lesions Using New Radiotherapy Techniques." OA Dermatology 1.1 (2013).

37 Solberg, Timothy D. Proc. of American Association of Physicists in Medicine 44th Conference, Montreal. 3 Oct. 2016.

38 Hardcastle, N., A. Davies, K. Foo, A. Miller, and Pe Metcalfe. "Rectal Dose Reduction with IMRT for Prostate Radiotherapy." Journal of Medical Imaging and Radiation Oncology 54.3 (2010): 235-48.

39 Podgorsak, Ervin D. "DOSIMETRIC PRINCIPLES, QUANTITIES AND UNITS." Radiation Oncology Physics: A Handbook for Teachers and Students. Vienna: International Atomic Energy Agency, 2005.

40 Papanikolaou, Nikos, Jerry J. Battista, Arthur L. Boyer, Constantin Kappas, Eric Klein, T. RockMackie, Michael Sharpe, and Jake Van Dyk. "Tissue Inhomogeneity Corrections for Megavoltage Photon Beams." American Association of Physicists in Medine 85 (2004).

41 Podgoršak, Ervin B. Radiation Physics for Medical Physicists. Berlin: Springer, 2009.

42 Fotina, Irina, Peter Winkler, Thomas Künzler, Jochen Reiterer, Isabell Simmat, and Dietmar Georg. "Advanced Kernel Methods vs. Monte Carlo-based Dose Calculation for High Energy Photon Beams." Radiotherapy and Oncology 93.3 (2009): 645-53.

43 Badusha, Ahamed, Mcgarry, Conor K. “Practical collimator optimization in the management of prostate IMRT planning: A feasibility study.” Journal of Radiotherapy in Practice. (2015).

44 Mayles, Philip, Alan E. Nahum, and Jean-Claude Rosenwald. Handbook of Radiotherapy Physics: Theory and Practice. New York: Taylor & Francis, 2007.

45 Feuvret, Loïc, Georges Noël, Jean-Jacques Mazeron, and Pierre Bey. "Conformity Index: A Review." International Journal of Radiation Oncology Biology Physics 64.2 (2006): 333 42.

46 Kairn, T., S. B. Crowe, and J. V. Trapp. "Correcting Radiation Survey Data to Account for Increased Leakage during Intensity Modulated Radiotherapy Treatments." Medical Physics 40.11 (2013).